

Biosorptive Performance of *Bacillus arsenicus* MTCC 4380 Biofilm Supported on Sawdust/MnFe₂O₄ Composite for the Removal of As(III) and As(V)

M. S. Podder¹ · C. B. Majumder¹

Received: 15 March 2016 / Accepted: 7 June 2016 / Published online: 6 July 2016
© Springer Science+Business Media Singapore 2016

Abstract One of the main environmental concerns of today is the occurrence of arsenic in wastewater. Targeting a solution for this problem, several efforts have been made towards research and application of cost-effective and effortlessly adaptable processes. The ability of a biofilm of *Bacillus arsenicus* MTCC 4380 supported on sawdust/MnFe₂O₄ composite to biosorb/bioaccumulate As(III) and As(V) was investigated in batch experiments. Optimum biosorption/bioaccumulation conditions were determined as a function of contact time and temperature. The equilibrium was achieved after about 220 min at 30 °C temperature. Nonlinear regression analysis was done to determine the best-fit kinetic model based on three correlation coefficients and three error functions and also to predict the parameters involved in kinetic models. The results showed that both Brouers–Weron–Sotolongo and Avrami models for both As(III) and As(V) were capable of providing realistic explanation of biosorption/bioaccumulation kinetic. Applicability of mechanistic models showed that the rate controlling step in the biosorption/bioaccumulation of both As(III) and As(V) was film diffusion rather than intraparticle diffusion. The estimated thermodynamic parameters ΔG^0 , ΔH^0 , and ΔS^0 revealed that biosorption/bioaccumulation of both As(III) and As(V) was feasible, spontaneous, and exothermic under examined conditions.

Electronic supplementary material The online version of this article (doi:10.1007/s41101-016-0007-x) contains supplementary material, which is available to authorized users.

✉ M. S. Podder
mou.chem11@gmail.com

C. B. Majumder
cbmajumder@gmail.com

¹ Department of Chemical Engineering, Indian Institute of Technology, Roorkee 247667, India

The activation energy (E_a) estimated from Arrhenius equation specified the nature of biosorption/bioaccumulation being ion exchange type. The effect of co-existing ions such as Cu²⁺, Zn²⁺, Bi³⁺, Cd²⁺, Fe³⁺, Pb²⁺, Co²⁺, Ni²⁺, Cr⁶⁺, and SO₄²⁻ at different concentrations was inspected.

Keywords Arsenic · Simultaneous biosorption and bioaccumulation · Kinetic · Mechanistic · Thermodynamic

Introduction

Arsenic and its compounds are considered extremely noxious environmental pollutants to which millions of people are exposed over the world through ingestion of polluted water [1]. Arsenic is released to the environment typically through natural processes, because of the occurrence of arsenical minerals, leaching and soil erosion, inputs from geothermal sources, and volcanic emissions in addition to a result of anthropogenic activities, such as combustion of fossil fuels, smelting, mining activities, use of arsenical pesticides, production of glassware, dyes, and drugs, etc. [1, 2]. Copper smelting causes a huge volume of wastewater having large amounts of inorganic compounds for instance heavy metals like lead, copper, zinc, iron, cadmium, bismuth, etc., and highly carcinogenic metalloid-like arsenic species, which poses a serious threat to man, flora, and fauna of our ecosystem by contaminating the natural water tables (ground water and surface water) in the vicinity [3].

Chronic uptake of arsenic by humans through polluted food and water may result in severe health hazard through the damage of major body organs, such as cancers of the lung, skin, kidney, liver, and urinary bladder and other problems such as loss of appetite, neurological disorders, and skin thickening (hyperkeratosis) [1, 4]. Arsenic exists in the natural

water mainly in inorganic species, arsenite (As(III)) and arsenate (As(V)). As(III) is the predominant arsenic form in reducing environment; whereas, As(V) is present mainly in oxidizing conditions. As(III) is considered 25–60-fold more poisonous than As(V) and inclines to be more mobile in the environment [2]. Because of these health hazards, in drinking water, the maximum contaminant level (MCL) of arsenic has been revised to 10 from 50 $\mu\text{g/L}$ by the World Health Organization (WHO) in 1993 [5] and the European Commission in 2003 [6].

Several techniques have been employed for scavenging of arsenic from water and wastewater, for example, chemical oxidation [7], membrane processes [8], adsorption [4, 9], ion exchange [10], and electrocoagulation [4], but none of them is extensively recognized due to cost or maintenance of the process.

The technical exploration for special methods has been focused on the utilization of biosorption or bioaccumulation process. Many microorganisms are renowned for being capable of removing metal ions from dilute aqueous solution and for accumulating them within their cell structure.

Bioaccumulation can be stated as the metabolism-dependent active uptake of toxins by living cells [11]. Biosorption is a metabolism-independent passive uptake of toxins by certain classes of dead/inactive biological materials or by materials derived from biological sources which may bind and accumulate toxins from aqueous solution [12]. Biofilms can be well established as microorganism communities attached to a surface [13]. There are four possible reasons for the formation of biofilm: defense (shield from risky situations), colonization (formation of biofilm as a mechanism for remaining in an encouraging position), community (use of cooperative profits), and default mode of growth. Bacteria exhibit the most of their usual activity by growing as a biofilm. It is probable that the existence of an appropriate substrate for attachment is all that is vital for encouraging formation of biofilm [14].

The mechanisms between biofilms and metal ions are well defined by Le Cloirec et al. and can be suggested as follows: bulk diffusion (diffusion of the metal ions remaining in solution to the external surface of the biofilm), external mass transfer (occurrence of mass transfer via the layer of high concentration round the biofilm), fast metal ion interactions with surface of solid and specifically with the bacterial wall (these interactions can be bioaccumulation, production of enzyme, biosorption on the bacterial surface, extracellular precipitation by metabolites formed by bacteria, oxidation and/or reduction, and extracellular complexation), gentle surface diffusion, diffusion into the biofilm prior to the interaction with bacteria, and last of all, interactions with bacteria existent inside the biofilm [13].

The objectives of the current study are (1) to characterize the prepared fresh biosorbent (SD/MnFe₂O₄ composite) and immobilized bacterial cells before and after metal loading with scanning electron micrograph (SEM), (2) to inspect the impact

of contact time as well as temperature for removing As(III) and As(V) from synthetically prepared copper smelting wastewater, (3) to evaluate the kinetics and mechanism of current biosorption/bioaccumulation process, (4) to scrutinize the thermodynamics of biosorption/bioaccumulation in order to identify the mechanism of biosorption/bioaccumulation process, (5) to investigate the effect of initial arsenic concentration on kinetics of biosorption/bioaccumulation, and (6) to study the influence of temperature on kinetics of biosorption/bioaccumulation.

Materials and Methods

Materials

Sawdust of *Syzygium cumini* (Jamun tree) was collected from a timber working shop situated near the campus of Indian Institute of Technology, Roorkee, India. All the chemicals and reagents were of analytical reagent grade and used without additional purification. Standards, matrix modifier, and wash solutions were prepared by deionized double distilled water. The stock solutions of As(III) and As(V) were purchased from Himedia Laboratories Pvt. Ltd. Mumbai India. All other necessary chemicals used in the experiments were purchased from Himedia Laboratories Pvt. Ltd. Mumbai India.

Microorganism and Growth Medium

The microorganism utilized was the arsenic-resistant bacterium *Bacillus arsenicus* (MTCC 4380; Microbial Type Culture Collection and Gene Bank (MTCC), Chandigarh, India). Culture media was prepared as per the guidelines of microbial-type cell culture (MTCC). Composition of growth medium and cultivation conditions are exhibited in Table S1 of the Electronic Supplementary Material.

Acclimatization

B. arsenicus MTCC 4380 was cultivated in a 250-mL flask containing 100 mL of the growth media with As(III) and As(V). The cultures were acclimatized to As(III) and As(V) individually exposing the culture in a series of shake flasks [14].

The bacterial inoculum was prepared by transferring a loop full of bacterial culture from the nutrient agar tubes to the flask containing sterilized growth media, incubated at 30 °C for 24 h with moderate agitation in an incubator cum orbital shaker. Then, the acclimatization of *B. arsenicus* MTCC 4380 in arsenic environment was carried out as follows:

After 24 h, the synthetic medium in the flask had turned milky specifying significant bacterial growth in the flask. Appropriate amount of arsenic (either As(III) or As(V)) was added into the flask having 100 mL sterilized growth media to

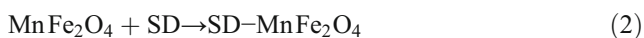
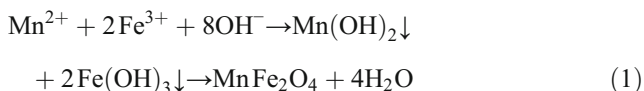
acquire a concentration of 50 mg/L of arsenic. Firstly, growth of *B. arsenicus* MTCC 4380 was inhibited and the growth started after 2 h. After 24 h of incubation at 30 °C, 5 mL of the arsenic-resistant bacterial inoculum was periodically added in a series of 250-mL flasks containing 100 mL of arsenic containing sterilized growth media (As(III) or As(V) concentration, 100, 200, 500, 800, 1000, 1200, 1500, and 1800 mg/L) under sterile conditions in a laminar hood chamber. After 24 h, another fresh growth media (As(III) or As(V) concentration, 2000 mg/L) was also inoculated with 5 mL of the last culture (As(III) or As(V) concentration, 1800 mg/L) to ensure that the bacteria was already adapted to both As(III) or As(V). For inoculum, a further subculturing was performed and all the inoculum transfers were done in exponential phase (OD value ~1 at 600 nm).

Methods

Biosorbent Preparation

Sawdust (SD) was washed to clean the adhering dirt, rinsed thoroughly with double distilled water, and finally heated in an air oven at 105 °C for 4 h; 25 g of dried SD were added into a 500-mL conical flask containing 250 mL of 0.5 M HCl solution; thereafter, it was shaken for 4 h at 120 rpm at 25 °C. The mixture was left overnight, and then it was filtered to separate SD which was repeatedly washed with double-distilled water to obtain neutral pH. Then, the biosorbents were dried at 110 °C for 3 h for removing moisture, cooled to room temperature, and kept in plastic bags for further usage.

SD/MnFe₂O₄ composites were prepared by chemical coprecipitation method with few modifications [15]. In this procedure, 11.52 g of acid-treated SD was mixed into 200 mL solution containing dissolved ferric(III) chloride (FeCl₃; 0.05 mol) and manganese(II) chloride (MnCl₂; 0.025 mol) at room temperature. The quantity of acid-treated SD was fixed for acquiring SD/MnFe₂O₄ mass ratios of 2:1. The solution temperature was increased to 60 °C under energetic magnetic stirring, and after that, 5 mol/L of NaOH solution was added drop by drop to the above mixture till the pH of the solution attained 11. Thereafter, agitation was carried out for 1 h. Then, the suspension was heated in a water bath at 100 °C for 4 h. After cooling, the prepared composite was constantly washed with double-distilled water to eliminate the contaminations (e.g., Na⁺, Cl⁻) accompanied with the processes. Afterward, as-prepared composite was collected from the washed solution by filtering the mixture and then was oven dried at 110 °C. The reaction ionic equation [16] is as follows:



Immobilization of Microbial Cells on the Biosorbent

To immobilize *B. arsenicus* MTCC 4380 on prepared SD/MnFe₂O₄ composite, initially, 95 mL culture media was inoculated with 5 mL of bacterial suspension of *B. arsenicus* MTCC 4380 from both As(III)- and As(V)-acclimatized 24-h-old culture. The flasks were incubated at 30 °C for the next 24 h with moderate shaking at 120 rpm. Then, immobilization of bacterial cell was performed by adding weighed amount of prepared SD/MnFe₂O₄ composite to the above suspension containing 24-h-old culture. Then, the flasks were again incubated at 30 °C for the next 24 h with moderate shaking at 120 rpm. Bacterial cell immobilization was established by observing a small amount of bacterial-treated SD/MnFe₂O₄ composite through scanning electron microscopy.

Characterization

The measurements of SEM were done for observing the surface morphologies of the *B. arsenicus* MTCC 4380 immobilized on the surface of SD/MnFe₂O₄ composite (i.e., immobilized bacterial cells) before and after biosorption/bioaccumulation process (SEM; LEO electron Microscopy, England). Infrared spectra of the unloaded and metal-loaded immobilized bacterial cells were acquired utilizing a Fourier transform infrared spectrometer (NICHOLET 6700, coupled with OMNIC software version 6.2).

Batch Experimental Studies and Analytical Methods

A medium with 1.0 g/L of beef extract and 2.0 g/L of yeast extract, 5.0 g/L of peptone, and 5.0 g/L of NaCl was utilized for the growth of the microorganism. The media was sterilized at 121 °C for 15 min, cooled to room temperature, inoculated with bacteria, and kept at 30 °C for 24 h with moderate agitation (120 rpm) in an incubator cum orbital shaker. All biosorption/bioaccumulation experiments were done by shaking optimum biosorbent dose of 0.9 g/L of the SD/MnFe₂O₄ composite (optimized in previous study) with 100 mL of *B. arsenicus* MTCC 4380 bacterial suspension as a test solution and required amount of arsenic (As(III) or As(V)) was supplemented to give a final requisite concentration of As(III) or As(V) at an optimum initial pH value around 7.0 (optimized in previous study) and at a preferred temperature in an incubator cum orbital shaker (REMI Laboratory instruments) at 120 rpm. 1.0 N NaOH and 1.0 N HCl solutions were used to adjust the initial pH of the solution using a digital pH meter (HACH® India).

To study the biosorption/bioaccumulation kinetics, batch experiments were conducted by contacting an optimum biosorbent dose (0.9 g/L) of the SD/MnFe₂O₄ composite with As(III) or As(V) solution of a fixed

concentration (50 mg/L) at a constant temperature of 30 °C at a range of contact time (5–500 min).

To inspect the impact of temperature on biosorption/bioaccumulation, batch experiments were done by contacting an optimum biosorbent dose (0.9 g/L) of the SD/MnFe₂O₄ composite with As(III) or As(V) solution of a fixed concentration (50 mg/L) at an optimum contact time of 220 min at a range of temperatures (20, 25, 30, 40, 45, and 50 °C).

To observe the influence of initial concentration on the kinetics of biosorption/bioaccumulation of both As(III) and As(V) by *B. arsenicus* MTCC 4380 immobilized on SD/MnFe₂O₄ composite, all batch experiments were performed by agitating 0.9 g/L of SD/MnFe₂O₄ composite with 100 mL of *B. arsenicus* MTCC 4380 bacterial suspension as a test solution supplemented with required amount of arsenic (As(III) or As(V)) to give final concentration As(III) or As(V) of 50, 100, 500, 1000, 1500, and 2000 mg/L at a constant temperature (30 °C).

To investigate the influence of temperature on the kinetics of biosorption/bioaccumulation of both As(III) and As(V) by immobilized bacterial cells, 0.9 g/L SD/MnFe₂O₄ composite was added to each round bottom flasks containing 50 mg/L *B. arsenicus* MTCC 4380 culture media as a test solution of As(III) or As(V). Experiments were conducted at three temperatures (30, 40, and 50 °C) by shaking the flasks.

The samples were withdrawn from the flasks through filtration using Whatman Filter paper (cat no. 1001 125; Remi Instruments Ltd., Mumbai, India) at predetermined time intervals for kinetic studies and after fixed contact time for thermodynamic studies. Then, the samples were centrifuged at 10000 rpm for 10 min for kinetic studies, a portion of filtrate was diluted with HNO₃ solution (10 %, v/v).

Interference Studies

The As(III) and As(V) binding capacity experiments were again done with synthetically prepared wastewater containing the co-existing ions commonly existing in copper smelting wastewater with arsenic solution. The effect of ions such as Cu²⁺, Zn²⁺, and SO₄²⁻ (100–2000 mg/L); Fe³⁺, Cd²⁺, and Bi³⁺ (10–500 mg/L); and Pb²⁺, Co²⁺, Ni²⁺, and Cr⁶⁺ (1–70 mg/L) on elimination of As(III) and As(V) were inspected.

Arsenic Quantification

The total arsenic was measured in a ThermoFisher Scientific iCE 3000 Series AA graphite furnace atomic absorption (GFAA) spectrometer, with Zeeman background correction (GF-AAS). A 0.5-nm slit width and a wavelength of 193.7 nm were chosen. An arsenic high-intensity hollow-cathode lamp was utilized for determining As <20 µg/L. Pyrolytic graphite-coated tubes with forked pyrolytic platforms were utilized. Argon (Ar) was utilized as a protective gas all throughout. To determine the dissolved arsenic, 8.0 mL of a

centrifuged sample was added to 1 mL of 1 % HNO₃ and 1.0 mL of chemical matrix modifier (50 g/L of nickel nitrate solution) in a flask. The prepared sample injected was 20 µL. All measurements were conducted at least in duplicate and on the basis of integrated absorbance.

Theoretical Background

With the goal of assessing biosorption capacity by mass balance, the amount of adsorbate molecules adsorbed per unit mass of biosorbent at time *t* (mg/g) was calculated:

$$q_t = (C_0 - C_t) \frac{V}{M} \quad (3)$$

The amount of adsorbate molecules adsorbed in terms of percentage was calculated as follows:

$$R_e(\%) = \frac{(C_0 - C_t)}{C_0} \times 100 \quad (4)$$

where *C*₀ and *C*_{*t*} are arsenic concentrations at time 0 and *t* (mg/L), respectively, *V* is the volume of the solution (mL), and *M* is the mass of biosorbent used (g).

Determining Adsorption Kinetic Parameters by Nonlinear Regression

The kinetic parameter sets are calculated by nonlinear regression due to the inherent bias affecting after linearization. This delivers a mathematically laborious method to estimate kinetic parameters utilizing the original kinetic equation [17]. Usually, Gauss–Newton methods or Levenberg–Marquardt-based algorithms [18] are used. The biosorption kinetic data of arsenic on the surface of immobilized bacterial cells were analyzed by nonlinear curve fitting analysis using professional graphics software package OriginPro (8.5.1 version) for fitting the kinetic models.

The optimization method needs the selection of a goodness-of-fit measure (GoFM) with the aim of esteeming the fitting of the kinetics to the experimental data. In the current study, six GoFM (residual sum of squares (SSE), reduced Chi-square test (reduced χ^2), coefficient of determination (R^2), adjusted *R*-square ($\overline{R^2}$), *R* value (*R*), and root-MSE value) were employed for assessing kinetic parameters using the OriginPro software by considering 95 % confidence interval (The details of GoFM are provided with the Electronic Supplementary Material).

The adjusted coefficient of determination ($\overline{R^2}$), which generally takes into account the number of variables and sample size in the model, is considered superior to the coefficient of determination (R^2), since it revises the overestimation by R^2 [19]. While dealing with small samples, specifically it is more exact than R^2 .

Adsorption Kinetic Modeling

There are many models for kinetics of biosorption at the interface of solid/solution. Fractional power model (FP), pseudo first order (PFO), and pseudo second order (PSO) are common empirical models. However, their major drawback is that they may simply define the kinetics of adsorption at some restrictive situations [20]. Elovich is a two-parametric semi-empirical model and FP, Ritchie second-order, and exponential (EXP) kinetic models are two-parametric empirical models to analyze kinetic data at near to equilibrium. As well as other empirical models for instance Avrami, modified pseudo second-order (MPSO) and mixed 1,2-order model (MOE) equations have been recommended for modeling the adsorption kinetics at the interface of solid/solution. These models are mainly three parametric equations. These new models are expected to describe the performance of a given biosorbent more accurately and to help gain insight in biosorption mechanism [21].

The prior kinetic models of adsorption at the interface of solid/solution can be generalized by taking into consideration the fractal-like methodology, i.e., time dependence of adsorption rate coefficient. A physical significance of the concept of fractal-like has been considered for adsorption kinetics on solid surfaces that are energetically heterogeneous. The fractal-like study demonstrates that the kinetics of adsorption at interface of the solid/solution in a real system with various kinds of surface sites and with various affinities for adsorption can be demarcated by a fractal-like methodology. Based on this study, the history of process can impact the process. Besides, the achieved rate coefficient of adsorption is a function of time. Table 1 presents representative kinetic models for a biosorptive reaction (The details of adsorption kinetic modeling are provided with the [Electronic Supplementary Material](#)).

Adsorption Mechanistic Modeling

The removal of adsorbate species from the liquid by the solid phase is occurring in three successive steps as follows [22, 23]. The three stages tangled in the mechanism of biosorption process are as follows:

- (i) Firstly, the adsorbate mass transfer from the aqueous phase on the biosorbent surface, i.e., film diffusion or surface diffusion takes place;
- (ii) Secondly, internal diffusion of adsorbate via either a pore diffusion model or homogeneous solid-phase diffusion model, i.e., particle diffusion occurs; and
- (iii) The third stage is the biosorption of adsorbate on the surface sites. Due to its very fast nature, it cannot be considered for the rate determining step.

So, as to know the rate controlling step, the following different models (Table 2) were applied using the experimental data of kinetic study (The details of mechanistic model equations are provided with the [Electronic Supplementary Material](#)).

Adsorption Thermodynamic Modeling

The entropy and Gibbs free energy parameters should be measured with the intention of deciding if the processes will happen spontaneously. Thermodynamic parameters, for example, ΔG^0 , ΔH^0 , and ΔS^0 can be calculated utilizing equilibrium constant while the temperature varies (Table 3), and their evaluation gives an insight into the possible nature of adsorption (The details of thermodynamic equations are provided with the [Electronic Supplementary Material](#)).

Adsorption Activation Energy

The adsorption activation energy (E_a) was calculated by considering the equilibrium constants under the different experimental conditions (Table 3) (The detailed equation is provided with the [Electronic Supplementary Material](#)).

Results and Discussion

Effect of Chemical Treatment on Biosorption

The acid-treated sawdust itself has the lower capacity to adsorb As(III) and As(V). Its main function was to provide a template with high specific area for MnFe_2O_4 loading. Untreated sawdust (SD), utilized in water treatment facilities, occupies mainly negatively charged surface due to hydroxyl group at neutral pH and therefore was not a good biosorbent for negatively charged/neutral arsenic. The hydroxyl groups can offer chemical reaction sites and adsorb iron and manganese ions to grow MnFe_2O_4 particles. The reason may be that the template can prevent MnFe_2O_4 particles from aggregating in biosorption process and enhance the effective biosorption area, resulting in the highly enhancement of biosorption capacity [4]. Loading of MnFe_2O_4 increased the positive charge density on the biosorbent surface by neutralizing negative surface charge and creating positive charge in its place [24]. Mondal et al. reported that impregnation of Ca on the surface of GAC also increased the positive charge on the surface of GAC and finally improved the adsorption capacity of GAC [25, 26]. By comparing the arsenic adsorption capacity of MnFe_2O_4 with and without the template in Table 4, it was observed that the adsorption capacities of MnFe_2O_4 loading on the acid-treated sawdust are much higher than the bare ones. Hereby, the introduction of acid-treated sawdust template can efficiently improve the adsorption capacity. The

Table 1 Adsorption kinetic models for biosorption

Sr. no.	Expression	Equation form	Remarks
1	Fractional power model (FP)	$q_t = k_{FP}t^v$	Based on adsorption capacity
2	Pseudo first-order model (PFO)	$q_t = q_e(1 - \exp(-k_{PFO}t))$	Based on adsorption capacity
3	Pseudo second-order model (PSO)	$q_t = \frac{(q_e^2 k_{PSO})t}{1 + (q_e k_{PSO}t)}$	Chemisorption and based on adsorption capacity and
4	Elovich model	$q_t = \left(\frac{2.3}{b_E}\right) \times \log\left(\frac{t+1}{a_E b_E}\right) - \left(\frac{2.3}{b_E}\right) \times \log\left(\frac{1}{a_E b_E}\right)$	Chemisorption
5	Avrami model	$q_t = q_e(1 - \exp(-(k_{AV}t)^{n_{AV}}))$	Multiple kinetic orders
6	Modified second-order model (MSO)	$q_t = q_e \left\{ 1 - \left(\frac{1}{\beta_{2R} + k_{2R}t} \right) \right\}$	Number of surface sites is two
7	Ritchie second-order model	$q_t = q_e \left\{ 1 - \left(\frac{1}{1 + k_{2R}t} \right) \right\}$	Adsorbent surface coverage is presumed to be zero
8	Exponential kinetic model (EXP)	$q_t = q_e(\ln(2.72 - 1.72 \exp(-k'_{EXP}t)))$	Exponential form of kinetic equation
9	Mixed 1,2-order model (MOE)	$q_t = q_e \frac{1 - \exp(-k_{MOE}t)}{1 - f_2 \exp(-k_{MOE}t)}$	A combined form of pseudo first- and second-order equations
10	Fractal-like mixed 1,2-order model (FMOE)	$q_t = \frac{q_e(1 - \exp(-k'_{1,0}t^\alpha))}{1 - f_{eq} \exp(-k'_{1,0}t^\alpha)}$	Time dependency of the rate coefficient
11	Fractal-like pseudo first-order model (FPFO)	$q_t = q_e(1 - \exp(-k'_{FPFO}t^\alpha))$	Time dependency of the rate coefficient
12	Fractal-like pseudo second order (FPSO)	$q_t = \frac{q_e^2 k'_{FPSO} t^\alpha}{1 + k'_{FPSO} q_e t^\alpha}$	Time dependency of the rate coefficient
13	Fractal-like exponential (FEXP)	$q_t = q_e \ln(2.72 - 1.72 \exp(-k'''_{EXP}t^\alpha))$	Time dependency of the rate coefficient
14	Brouers–Weron–Sotolongo model (BWS)	$q_t = q_e \left(1 - \left(1 + (n_{BWS}-1) \left(\frac{t}{\tau_{n_{BWS},\alpha}} \right)^\alpha \right)^{-1/(n_{BWS}-1)} \right)$	Complex nature of adsorption

Table 2 Adsorption mechanistic models for biosorption

Sr. no.	Expression	Equation form	Remarks
1	Weber and Morris model	$q_t = k_{int}t^{0.5} + C_{int}$	Intradiffusion
2	Rate-limiting step	$\ln\left(1 - \frac{q_t}{q_e}\right) = \ln\left(\frac{6}{\pi^2}\right) - \left(\frac{D_s \pi^2}{r^2}\right) t$	Based on diffusion
3	Dumwald–Wagner model	$\log(1 - F^2) = \frac{-k_{DW}}{2.303} t$	Intradiffusion
4	Richenberg model	$F \text{ values } > 0.85$ $B_b t = -0.4977 - \ln(1 - F)$ $F \text{ values } < 0.85$ $B_b t = \left(\sqrt{\pi} - \sqrt{\pi - \frac{\pi^2 F}{3}} \right)$	Based on diffusion
5	McKay plot	$\ln(1 - F) = -k_M t$	Film diffusion
6	Bangham’s model	$\log\left(\log\left(\frac{C_0}{C_0 - q_m}\right)\right) = \log\left(\frac{k_b m}{2.303 V}\right) + \alpha_b \log(t)$	Intradiffusion
7	Diffusion coefficient	$t_{(1/2)} = \frac{0.030r^2}{D_p}$ $t_{(1/2)} = \frac{0.230r\delta}{D_f} \times \frac{C_s}{C_e}$	Based on diffusion
14	Diffusivity model	$F = 1 - \left(\frac{6}{\pi^2}\right) \sum_{m_b} \left(\frac{1}{m_b^2}\right) \exp\left(-\frac{D_e t \pi^2 m_b^2}{r^2}\right)$	Chemisorption

Table 3 Thermodynamic equations and their parameters

Sr. no.	Expression	Equation form	Remarks
1	Gibbs free energy	$\Delta G^0 = -RT \ln K_d$ where $k_d = \frac{q_e}{C_e}$ (80)	Free energy change
12	van't Hoff	$\ln(k_d) = -\frac{\Delta H^0}{RT} + \frac{\Delta S^0}{R}$ where $k_d = \frac{q_e}{C_e}$	Enthalpy change Entropy change
14	Arrhenius	$\ln k_{\text{PSO}} = -\frac{E_a}{RT} + \ln A$	Apparent activation energy

reason may be that the template can prevent MnFe_2O_4 particles from aggregating in adsorption process and enhance the effective adsorption area, resulting in the highly enhancement of adsorption capacity. A similar finding has been found for the loading of Fe_3O_4 on pure wheat straw [27].

Effect of Contact Time

Figure 1 shows the effect of contact time on the percent removal of As(III) and As(V) utilizing immobilized bacterium. The time needed to attain equilibrium for removal of both As(III) and As(V) was 220 min. With further increase in time, no remarkable improvement was observed in removing arsenic. So, further biosorption/bioaccumulation studies were done for a contact time of 220 min.

From the outcomes, it is further clear that in all the systems, the saturation time are not influenced by the adsorbate concentration in the solution. The change in the rate of removal might be due to the fact that initially all sites of surfaces of immobilized bacterial cells are easily accessible and also the concentration gradient of adsorbate is very high. At optimum pH, the fast kinetics of interaction of adsorbate-immobilized bacterial cells might be accepted to increase availability of the active sites of the surface of immobilized bacterial cells. So, the scavenging of adsorbate was rapid in the early stages and gradually decreases with the interval of time until equilibrium in each case. The reduction in removal of metal ion at the later stage of the process was due to the decreasing of concentration of metal ions [28]. Furthermore, the characteristic of the equilibrium time curve exhibited that the SBB process approaches

the equilibrium in a short span of time [29]. So, the curves found were single, smooth, and continuous, leading to equilibrium and suggested the probability of monolayer coverage of the adsorbate on the surface of immobilized bacterial cells [30].

Biosorption Kinetic Studies

Information on the kinetics of adsorbate uptake is important to find optimum operating conditions for full-scale batch process. As a nonlinearizable kinetic model and with the determination of comparing its fitting capability with the previous considered models, a nonlinear regression analysis was carried out to 14 adsorption kinetic model. Table S2 of the Electronic Supplementary Material shows the values of kinetic constants of all the models for the biosorption/bioaccumulation of both As(III) and As(V) by immobilized bacterial cells. The results exhibited that there was no notable relationship between the kinetic data for both As(III) and As(V) (Fig. S1) with low correlation coefficients and high error values signifying that these models (fractional power, pseudo first order, Elovich, and exponential) are not suitable in the present case.

On the basis of the maximum correlation coefficients (R and R^2) and the lowest error values (reduced χ^2), the superior and perfect fitting of the experimental results was observed using Brouers–Weron–Sotolongo for both As(III) and As(V) (Fig. S1) among all the tested kinetic models; whereas on the basis of maximum correlation coefficients ($\overline{R^2}$) and the lowest error values (SSE and root-MSE), the better and perfect demonstration of the experimental results was attained using

Table 4 Comparison of the percent removal of As(III) and As(V) using different adsorbents/biosorbents

Adsorbents	Operating conditions	% removal of As(III)	% removal of As(V)
<i>B. arsenicus</i> MTCC 4380 immobilized on surface of SD/ MnFe_2O_4 composite	C_0 , 50 mg/L; M , 4 g/L; pH, 7.0; T , 30 °C; t , 90 min	83.043	89.462
SD/ MnFe_2O_4 composite	C_0 , 50 mg/L; M , 4 g/L; pH, 7.0 (As(III)) and 4.0 (As(V)); T , 30 °C; t , 90 min	86.957	89.692
Acid-treated SD	C_0 , 50 mg/L; M , 4 g/L; pH, 7.0 (As(III)) and 4.0 (As(V)); T , 30 °C; t , 90 min	78.261	82
Bare MnFe_2O_4	C_0 , 50 mg/L; M , 4 g/L; pH, 7.0 (As(III)) and 4.0 (As(V)); T , 30 °C; t , 90 min	66.08696	57.38462

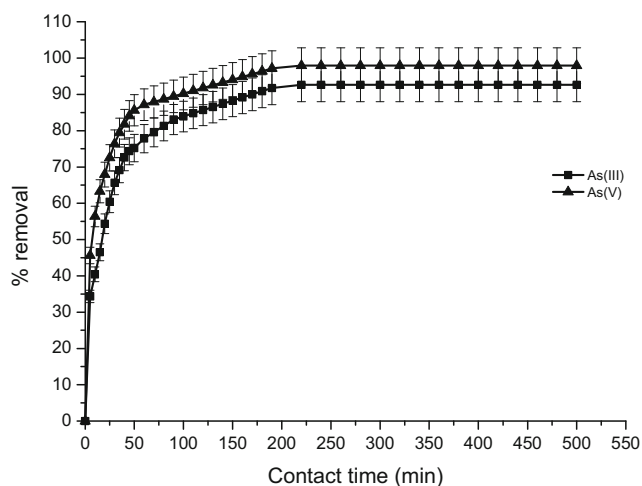


Fig. 1 Effect of contact time on As(III) and As(V) removal in SBB studies (C_0 , 50 mg/L; T , 30 °C; pH, 7.0; M , 0.9 g/L). Error bars represent means \pm standard errors from the mean of duplicate experiments

Avrami kinetic model (Fig. S1) among all the well-known kinetic models for both As(III) and As(V).

The equilibrium uptake (q_e ; 51.72 and 54.975 mg/g for As(III) and As(V), respectively), acquired from Brouers–Weron–Sotolongo model was closely in line with the experimental value (51.449 and 54.402 mg/g for As(III) and As(V), respectively). Returning to the theory beyond the best fitting model (i.e., BWS), the biosorption/bioaccumulation phenomenon of both As(III) and As(V) on the surface of immobilized bacterial cells would be controlled by chemisorption interactions type, enlightening that the rate governing step might be chemical adsorption, including valency forces by means of exchange or sharing of electrons between As(III) or As(V) anions and immobilized bacterial cells. Also, BWS model expresses another remarkable data which is the time important to adsorb half the maximum amount ($\tau_{nBWS, \alpha}$). As presented in Table S2 of the Electronic Supplementary Material, with respect to initial arsenic concentration, 23.226 and 12.45 min (the lowest value) were sufficient to immobilized bacterial cells to attain half of the As(III) and As(V) uptake capacities, respectively, which is significant in addition to valuable parameter for calculating the reaction speed. As for BWS model itself, it has a good fitting behavior and more implicitly, it expresses such quality data (i.e., adsorption capacity nearest to experimental value ($q_{e(BWS)}$) and the time of half reaction ($\tau_{nBWS, \alpha}$)), which are valued aimed at industrial treatment design purposes [31].

Avrami exponent (n_{AV} ; 0.599 for As(III) and 0.49 for As(V)) is a fractionary number connected with the possible variations of the biosorption/bioaccumulation mechanism that happens all over the biosorption/bioaccumulation process [32]. In place of following only an integer-kinetic order, the mechanism of biosorption/bioaccumulation could follow multiple kinetic orders that are altered throughout the contact of the adsorbate with immobilized bacterial cells [32]. n_{AV} is a resultant of the multiple kinetic order of the biosorption/bioaccumulation procedure.

On the basis of good correlation coefficient (R , R^2 , and $\overline{R^2}$) and low error values (SSE, reduced χ^2 , and root-MSE), it can be confirmed that other kinetic models, for example, pseudo second order, modified second order, Ritchie second order, fractal-like pseudo second order, and fractal-like mixed 1,2 order, fractal-like exponential models also exhibited good fitting of biosorption/bioaccumulation kinetic data for both As(III) and As(V) on the surface of immobilized bacterial cells.

The value of good correlation coefficients (R , R^2 , and $\overline{R^2}$) and low error values (SSE, reduced χ^2 , and root-MSE) for pseudo second-order model forecasts that mechanism of biosorption/bioaccumulation is a chemisorption type.

It is understood that the mixed 1,2-order rate equation is linear in the Lagergren coordinates (i.e., it behaves like the first-order equation) near to the equilibrium and somewhat in the initial portion of the experiment. Precisely, we may conclude that it contains two linear segments connected with a curved one. Actually, the second-order equation shows linear behavior in the initial portion of the experiment also, though the linear section is quite short. On the other hand, MOE may be treated as a Langmuir equation for energetically homogeneous surfaces or as purely empirical equation for energetically heterogeneous surfaces.

The vital assumption of modified second-order model was that a number of surface sites (n_R) are used by each adsorbate. It was supposed that the pre-adsorbed stage occurred on immobilized bacterial cells biosorption/bioaccumulation.

The vital supposition of the Ritchie second-order model was that one adsorbate was adsorbed on two surface sites. It was supposed that the pre-adsorbed stage has not occurred on immobilized bacterial cell biosorption/bioaccumulation [33]. The biosorbent surface coverage has been typically presumed to be zero.

In case of fractal-like models (fractal-like pseudo first order, fractal-like pseudo second order, fractal-like exponential, and fractal-like mixed 1,2 order), the biosorption/bioaccumulation rate coefficient is considered a function of time by using the fractal-like idea. One of the probable physical significances of fractal-like kinetics was that the biosorption/bioaccumulation of As(III) and As(V) occurred at solid/solution interface. In this approach, it was showed that by passing time, various paths for biosorption/bioaccumulation of As(III) and As(V) on surface appears [34].

Final Remarks on Biosorption/Bioaccumulation Kinetic Studies

The value of correlation coefficient (R and R^2) and error value (reduced χ^2) for Brouers–Weron–Sotolongo model was better than achieved using the other kinetic model for both As(III) and As(V), indicating a complex mechanism of biosorption/bioaccumulation. But based on the obtained correlation

coefficient ($\overline{R^2}$) and error values (SSE and root-MSE), the Avrami model showed the best fit to the biosorption/bioaccumulation kinetic data of both As(III) and As(V) among all the models, indicating that the mechanism of biosorption/bioaccumulation models followed multiple kinetic order. So, the kinetics of As(III) and As(V) biosorption/bioaccumulation using immobilized bacterial cells as a biosorbent can be well elucidated by Brouers–Weron–Sotolongo as well as Avrami kinetic models.

Among the models, pseudo second-order model also possessed a good fitness with experimental kinetic data. This tendency comes as a suggestion that the rate-limiting step in biosorption/bioaccumulation of arsenic (either As(III) or As(V)) are chemisorption involving valence forces through the sharing or exchange of electrons between immobilized bacterial cells and arsenic (either As(III) or As(V)) ions [35], complexation, coordination, and/or chelation [36].

It is important to find the rate at which As(III) or As(V) is biosorbed/bioaccumulated on the surface of immobilized bacterial cells, which is vital for designing the fixed bed biosorption column. Using the biosorption/bioaccumulation rate, kinetic constants are evaluated to define the equilibrium capacity of immobilized bacterial cells and mass transfer coefficient at various aqueous phase concentrations. Amount of As(III) or As(V) biosorbed/bioaccumulated on solid surface is calculated using the kinetic equation, which is vital for esteeming the concentration of the aqueous phase in fixed bed column operation. The key design factors of fixed bed adsorption column, the breakthrough time in addition to the shape of breakthrough curve are dependent on biosorption/bioaccumulation rate. For the faster biosorption/bioaccumulation rate, breakpoint time is attained earlier and the breakthrough curve shape is also steeper.

The descriptive models from the best to worst for As(III) and As(V) were sorted according to GoFM values and shown in Tables S3 and S4, respectively.

So, at this point, the fitting “ambiguity” influenced by R , R^2 , $\overline{R^2}$, SSE, reduced χ^2 , and root-MSE were for both As(III) and As(V), because R , R^2 , and reduced χ^2 established the Brouers–Weron–Sotolongo as best fitting model whereas $\overline{R^2}$, SSE, and root-MSE showed that the Avrami kinetic model is the best fitting model. So, for overcoming this doubt, it would be modest and practical to compare the theoretically evaluated q_e values with the experimental ones.

According to correlation coefficient $\overline{R^2}$ values the fitness of the models for all kinetic models are almost equivalent to each other. So, based on equivalent adsorption capacity, the orders followed by the models in decreasing manner are shown in Table S5. From Table S5, it can be concluded that on the basis of equivalent biosorption/bioaccumulation capacity, fractal-like pseudo second-order kinetic model is the best fitting model for both As(III) and As(V) owing to the highest value.

Biosorption Mechanistic Studies

Intraparticle Diffusion Model

Outcomes of intraparticle model for both As(III) and As(V) are shown in Table 5. Figure S2 indicated the multi-linear nature of intraparticle model. As the plot did not pass through the origin, so intraparticle diffusion was not the only rate governing step. So, there were three processes leading the rate of biosorption/bioaccumulation; however, only one was rate controlling in any certain time range. The intraparticle diffusion rate constant k_{int2} for both As(III) and As(V) was valued from the slope of the second linear portion (Fig. S2; Table 5). The multi-linear curve of the intraparticle model with intercept C_{int2} indicated the fact that both intraparticle diffusion of adsorbate through the mesoporus openings filled with liquid and film/external mass transfer across the thickness of boundary layer were the rate governing steps in the biosorption/bioaccumulation of both As(III) and As(V) kinetics on the surface of immobilized bacterial cells. The value of intercept C_{int} acquired through the model conveyed the value of thickness of boundary layer of liquid surrounding the immobilized bacterial cells [37].

The explanation of the random data points found in Fig. S2 and Table 5 specified that intraparticle mechanistic model had been appropriate to cost-effectively and competently describe the biosorption/bioaccumulation of both As(III) and As(V) on the surface of immobilized bacterial cells in terms of linear regression coefficient adjusted R -square ($\overline{R^2}$), ranging between 0.927 and 0.993 in both case. Larger value of intercepts achieved for second linear portion, i.e., C_{int2} suggested that the film diffusion had played a vital role as the rate governing step [38].

Determination of Rate-Limiting Step

The values of the film diffusion coefficient D_1 and the pore diffusion coefficient D_2 for both As(III) and As(V) are revealed in Table 5. The high negative exponential of almost nearest values specified that both pore diffusion and film diffusion had controlled the mechanism of biosorption/bioaccumulation for both As(III) and As(V).

Dumwald–Wagner Model

The plot (Fig. S3) of $\log(1 - F^2)$ versus t has delivered almost linear curves (≥ 0.947) for the scavenging of both As(III) and As(V) by immobilized bacterial cells, respectively, but did not pass through the origin, suggesting that the diffusion of adsorbate into pores of the immobilized bacterial cells was not the only rate-limiting step in both cases. Table 5 displays the evaluated results of Dumwald–Wagner model. In the current study, the linearity of the plots intersected the origin of

Table 5 Mechanistic constants of studied models for As(III) and As(V) biosorption/bioaccumulation on the surface of immobilized bacterial cells

Mechanistic models	Parameters	Values for As(III)	Values for As(V)
Intraparticle diffusion model	k_{int1} (mg/g min ^{0.5})	6.056	6.511
	C_{int1} (mg/g)	2.626	6.750
	k_{int2} (mg/g min ^{0.5})	1.268	0.932
	C_{int2} (mg/g)	33.478	40.877
	$\overline{R^2}_1$	0.983	0.927
	$\overline{R^2}_2$	0.983	0.993
Determination of rate-limiting step	D_1 (cm ² /s)	1.447E-05	1.098E-05
	D_2 (cm ² /s)	6.436E-06	6.133E-06
Dumwald–Wagner model	k_{DW} (1/min)	0.017	0.016
	$\overline{R^2}$	0.961	0.947
Richenberg model	$\overline{R^2}$	0.964	0.948
	k_{M1} (1/min)	0.032	0.037
McKay plot	k_{M2} (1/min)	0.018	0.017
	$\overline{R^2}_1$	0.967	0.941
	$\overline{R^2}_2$	0.916	0.880
	k_b (L/g)	20.828	32.849
Bangham's model	α_b	0.494	0.460
	$\overline{R^2}$	0.985	0.987
	D_p (cm ² /s)	1.114E-07	1.713E-07
Diffusion coefficient	D_f (cm ² /s)	1.958E-07	1.072E-06
	D_e (m ² /s)	5.949E-14	5.875E-14
Diffusivity	$\overline{R^2}$	0.964	0.948

coordinates; so, film diffusion process was the rate controlling step.

Richenberg Model or Boyd Plot

The consequences of the corresponding model for both As(III) and As(V) are exhibited in Table 5 and Fig. S4, respectively. From the plots of $B_b t$ versus t , it was detected that the plots had dynamic linear form with a correlation coefficient adjusted R -square ($\overline{R^2}$) of 0.964 for As(III) and 0.948 for As(V) at studied temperature but did not pass through origin which had selected the ongoing biosorption/bioaccumulation processes to be governed by film diffusion mechanism.

Film Diffusion Mass Transfer Rate Equation or McKay Plot

The values achieved for $\ln(1 - F)$ as a function of time t , were plotted in Fig. S5 for As(III) and As(V), respectively, and the results of the respective model for both As(III) and As(V) are revealed in Table 5. The rate constant of the initial fast process (k_{M1}) was evaluated from the slope of the first straight line

(Fig. S5). As can be understood from Fig. S5, the rate constant of the slow process (k_{M2}) was attained from the slope of the second linear portion. It is clear that the initial fast process was directed by film diffusion. Also the values of k_{M2} are smaller than the values of k_{M1} for both As(III) and As(V). So, the acquired values of k_{M2} were evidence of a pore diffusion mechanism in the second stage of the biosorption/bioaccumulation [39]. The existence of two straight lines for both As(III) and As(V) indicated that two processes, i.e., film diffusion and pore diffusion had involved in these processes.

The plots were about linear for both As(III) and As(V), but it did not yield perfect linearity. So, pore diffusion was not the rate controlling step. In the current study film diffusion was the rate governing step.

Bangham's Model

The results of the respective model for both As(III) and As(V) are exposed in Table 5 and Fig. S6. The goodness of fit of curve for Bangham's model was connected in terms of correlation coefficient adjusted R -square ($\overline{R^2}$). Values of Bangham

parameters k_b and α are 20.828 L/g and 0.494 for biosorption/bioaccumulation of As(III) and 32.849 L/g and 0.46 for biosorption/bioaccumulation of As(V) with a correlation coefficients of 0.984 and 0.987, respectively. The double logarithmic plot (Fig. S6) for As(III) and As(V), respectively, as specified by the above equation did not return perfect linear curves, and some data were dispersed ($\overline{R^2} \leq 0.987$) for the removal of As(III) and As(V) by immobilized bacterial cells illuminating that the diffusion of adsorbate within pores of the immobilized bacterial cells was not only the rate governing step [40], film diffusion also had impact on the rate-limiting step.

Determination of Diffusion Coefficient

The D_p and D_f values for As(III) were 1.11×10^{-7} and 1.96×10^{-7} cm²/s, respectively. Likewise, these values for As(V) were 1.71×10^{-7} and 1.07×10^{-6} cm²/s, respectively (Table 5).

Thus, in the current system, pore diffusion was not the only rate governing step for both As(III) and As(V). For As(III), the value of D_f (1.96×10^{-7} cm²/s) falls within the range of 10^{-6} and 10^{-8} cm²/s, and for As(V), the D_f value (1.07×10^{-6} cm²/s) is also in the range. So, it was noticed that the film diffusion had been the rate controlling step for both As(III) and As(V).

Higher value of D_f of As(V) than that of As(III) was owing to the presence of As(V) as totally positively charged species and As(III) as usually neutral species at the experimental pH. Due to negative charge of As(V), it was freely transported from the bulk solution to generally the positively charged immobilized bacterial cells and acquired biosorbed/bioaccumulated on the active sites of surface of immobilized bacterial cells in place of the interior pores.

Determination of Diffusivity

From the slope $\pi^2 D_e / r^2$ of the plot of $\ln(1/(1 - F^2))$ versus t (Fig. S7; Table 5), the value of diffusion coefficient (D_e) as assessed, was detected to be 5.95×10^{-14} and 5.87×10^{-14} m²/s for As(III) and As(V) biosorption/bioaccumulation on the surface of immobilized bacterial cells, respectively. For the current study, the value of D_e lies within the range of 10^{-9} to 10^{-17} m²/s, so the system was chemisorption system. The values of the diffusion coefficient, D_e fell well within the magnitudes reported in literature [41].

Final Remarks on Biosorption/Bioaccumulation Mechanistic Studies

The above-considered models for biosorption/bioaccumulation of both As(III) and As(V) specified that two processes, i.e., film diffusion (diffusion of adsorbate through the solution to the

external surface of biosorbent or boundary layer diffusion of adsorbate) and pore diffusion (diffusion of the adsorbate from the surface film into the pores) were involved in the current biosorption/bioaccumulation processes for both As(III) and As(V) and pore diffusion was not the only rate controlling step. Usually, film diffusion controlled the rate governing step in both cases. The uptake of arsenic (As(III) or As(V)) species from the liquid to the solid phase was carried out in three consecutive steps [23]. Firstly, film diffusion occurred. Secondly, pore diffusion took place. The third step is the biosorption, which is being very rapid in nature and cannot be taken into account for the rate determining [22].

Effect of Temperature

The temperature has two main influences on the biosorption/bioaccumulation process. Temperature essential for the biosorption/bioaccumulation system commands the biosorption/bioaccumulation as endothermic or exothermic. Increasing the temperature is familiar to raise the rate of diffusion of the adsorbate, due to the reduction in the viscosity of the solution. Besides, changing the temperature will alter the equilibrium biosorption capacity of the immobilized bacterial cells for a specific biosorbent [42].

The effect of temperature on the removal efficiency of As(III) and As(V) was inspected in the range of 20–50 °C during the equilibrium time. The consequences of influence of temperature have been exposed in Fig. 2. It was observed from Fig. 2 that with a little increase in temperature from 20 to 30 °C, the biosorption/bioaccumulation of arsenic (either As(III) or As(V)) ions on immobilized bacterial cell surface increased. After 30 °C temperature, the removal of arsenic (As(III) or As(V)) ions by immobilized bacterial cell

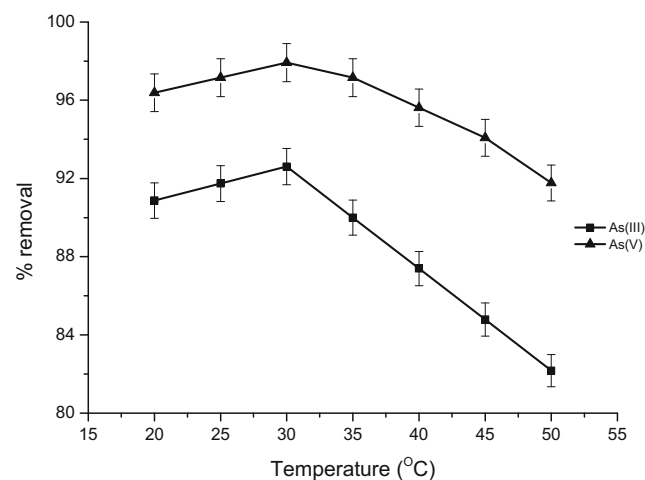


Fig. 2 Effect of temperature on As(III) and As(V) removal in SBB studies (C_0 , 50 mg/L; pH, 7; M , 0.9 g/L; t , 220 min). Error bars represent means \pm standard errors from the mean of duplicate experiments

decreased with the increase in temperature. For As(III) and As(V), percent removal decreased from 92.609 to 82.174 % and from 97.923 to 91.769 %, respectively, with increase in temperature from 30 to 50 °C.

The favorable temperature for the growth of *B. arsenicus* MTCC 4380 is 30 °C [43]. The result specified that the highest removal was at a temperature of 30 °C in biosorption/bioaccumulation system. Further increase in temperature resulted in lower scavenging efficiency for arsenic removal in biosorption/bioaccumulation system.

This can also be clarified by the exothermicity of the biosorption/bioaccumulation process. Temperature influences the interaction between the biomass and the metal ions, generally by impacting the stability of the metal-sorbent complex and the ionization of the cell wall moieties [44]. The temperature of the biosorption solution could be vital for energy-dependent mechanisms in metal binding process [45]. Energy independent mechanisms are less expected to be influenced by temperature because the processes responsible for biosorption are mainly physico-chemical in nature [46, 47]. The results acquired in the current study indicated that the metal ion sorption in SBB system was exothermic. Kacar et al. [46] and Ozdemir et al. [47] reported in their work about the exothermic behavior of metal ion sorption on the bacterial surface. The authors correlated their research outcomes as an energy-independent mediated sorption of metal ions.

This can also be clarified by the spontaneity of the biosorption/bioaccumulation process. Initial rise in removal efficiency up to 30 °C is mainly because of the rise in collision frequency between biosorbent and adsorbate. Further rise in temperature (>30 °C) caused in lower removal efficiency for arsenic removal by immobilized bacterial cells. This reduction in scavenging efficiency might be owing to many factors: the relative increase in the dodging tendency of the arsenic ions

from the solid biosorbent phase to the bulk liquid phase; deactivating immobilized bacterial cells or destructing some active sites on the surface of immobilized bacterial cells due to bond ruptures [48] or owing to the weakening of biosorptive forces between the adsorbate species and the active sites of the immobilized bacterial cells and also between the adjacent molecules of adsorbed phase for high temperatures or movement of biosorbents with more speed, so, lower interaction time with the biosorbent active sites was available for them [49].

Biosorption Thermodynamic Studies

The estimated values of the thermodynamic parameters from the plot of $\ln k_d$ versus $1/T$ (Fig. 3) are shown in Table 6. The equilibrium constant k_d was evaluated while the temperature was altered between 20 and 50 °C for both As(III) and As(V). The maximum scavenging of adsorbate was achieved at 30 °C in both cases. The removal efficiency primarily rose with rising the temperature from 20 to 30 °C. Then, it reduced with rising the temperature from 30 to 50 °C. The ΔH^0 values attained for the biosorption/bioaccumulation of both As(III) and As(V) were negative due to the exothermic nature of the biosorption/bioaccumulation process. The value achieved for As(V) biosorption/bioaccumulation was more than the value achieved for As(III). A negative value of ΔG^0 specified the spontaneous nature of the biosorption/bioaccumulation process; however, the negative value of ΔS^0 presented a decrease in the randomness at the solid/solution interface during the biosorption/bioaccumulation process [50]. Higher negative value of ΔG^0 at a temperature of 30 °C, as was achieved in the study, concluded more driving force for biosorption/bioaccumulation at 30 °C [51]. The values of ΔG^0 achieved in the current research were between -22.68 and -24.04 and -25.08 and -27.37 kJ/mol for As(III) and As(V), respectively.

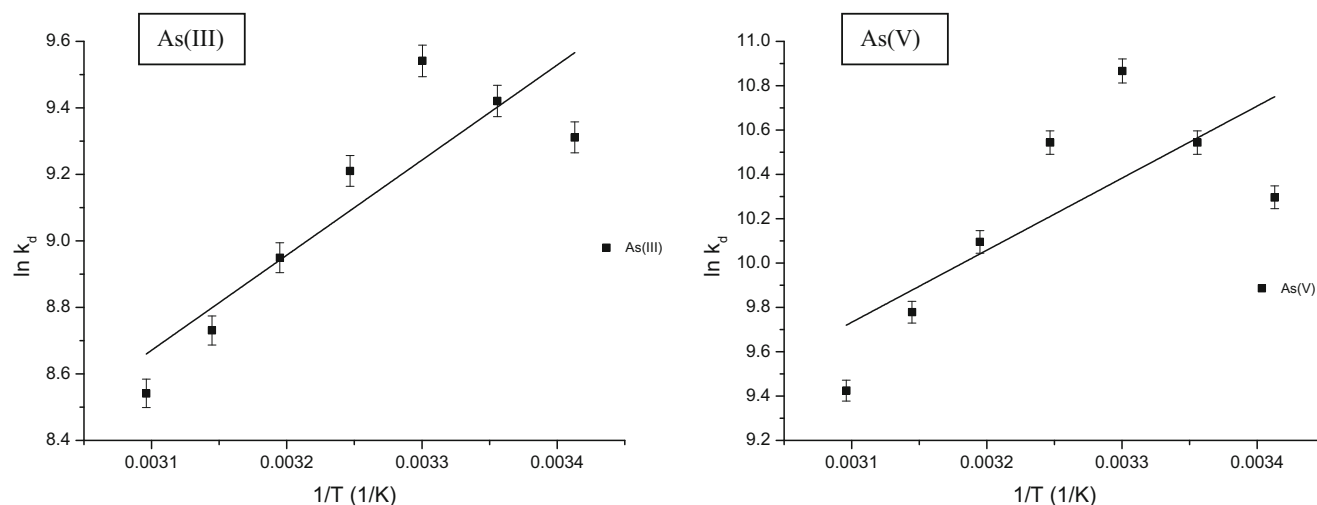


Fig. 3 Thermodynamic modeling of As(III) and As(V) biosorption/bioaccumulation on the surface of immobilized bacterial cells (T , 20–50 °C; C_0 , 50 mg/L; pH, 7.0; M , 0.9 g/L; t , 220 min). Error bars represent means \pm standard errors from the mean of duplicate experiments

Table 6 Thermodynamic constants for As(III) and As(V) biosorption/bioaccumulation on the surface of immobilized bacterial cells

Inorganic form	T (K)	$-\Delta G^0$ (kJ/mol)	$-\Delta H^0$ (kJ/mol)	$-\Delta S^0$ (J/mol K)
As(III)	293	22.681	23.768	0.002
	298	23.340		
	303	24.036		
	308	23.585		
	313	23.288		
	318	23.083		
	323	22.937		
As(V)	293	25.082	27.029	0.003
	298	26.122		
	303	27.374		
	308	26.999		
	313	26.271		
	318	25.853		
	323	25.309		

Thus, it indicated that the mechanism of current biosorption/bioaccumulation process had happened via ion exchange and/or surface complexation mechanism.

Effect of Initial Arsenic Concentration on Biosorption/Bioaccumulation Kinetics

To inspect the influence of initial concentration on kinetic studies, a series of contact time experiments for both As(III) and As(V) was performed at various initial concentration (50–2000 mg/L) at temperature of 30 °C. Figure S8 shows the contact time essential for both As(III) and As(V) with an initial concentration of 50–1000 mg/L for attaining equilibrium at 220 min. However, for both As(III) and As(V) with higher initial concentration (>1000–2000 mg/L), higher equilibrium time of 300 min was needed. As can be decided from Fig. S8, the amount of the biosorbed/bioaccumulated As(III) and As(V) on the surface of immobilized bacterial cells changed with time and at some point in time achieved a constant value beyond which no more As(III) or As(V) was scavenged from solution. At the moment, the amount of both As(III) and As(V) desorbing from the biosorbent was in a state of dynamic equilibrium with the amount of the both As(III) and As(V) being biosorbed/bioaccumulated on the surface of immobilized bacterial cells. The time vital for achievement of this state of equilibrium is called the equilibrium time. Thus, the rate of biosorption/bioaccumulation reduced with time till it tended to a plateau owing to the constant reduction in the concentration driving force.

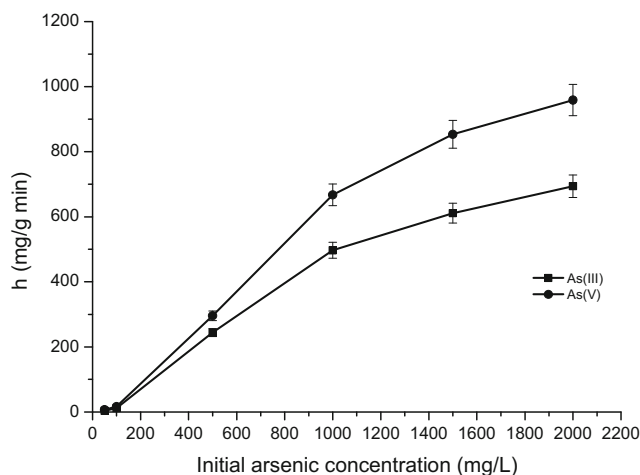


Fig. 4 Determination of the initial sorption rate for biosorption/bioaccumulation of As(III) and As(V) on the surface of immobilized bacterial cells (C_0 , 50–2000 mg/L; t , 5–500 min; pH, 7; M , 0.9 g/L; T , 30 °C). Error bars represent means \pm standard errors from the mean of duplicate experiments

Determination of Initial Sorption Rate

From Fig. 4 and Table 7, it is noted that the pseudo second-order rate constants (k_{PSO}) were detected to decrease and the initial sorption rates (h) were agreed to rise with higher initial concentration of both As(III) and As(V). The initial sorption rate was larger for higher initial As(III) and As(V) concentrations as the resistance to uptake both As(III) and As(V) decreased as the mass transfer driving force was enhanced.

The estimated $q_{e(PSO)}$ values confirmed just appropriate with the experimental data, and high correlation coefficient (R , R^2 , and $\overline{R^2}$) and low error values (SSE, reduced χ^2 , and root-MSE) revealed that the model can be utilized for the

Table 7 Initial sorption rate for As(III) and As(V) biosorption/bioaccumulation on the surface of immobilized bacterial cells

Inorganic form	Concentration (mg/L)	k_{PSO} (g/mg min)	h (mg/g min)
As(III)	50	1.350E-03	3.864
	100	1.160E-03	11.813
	500	1.030E-03	244.083
	1000	6.735E-04	497.025
	1500	4.547E-04	611.120
	2000	3.696E-04	694.031
As(V)	50	2.210E-03	6.755
	100	1.380E-03	16.554
	500	1.220E-03	295.792
	1000	7.698E-04	667.233
	1500	5.146E-04	853.540
	2000	4.052E-04	958.904

whole biosorption/bioaccumulation process and allowed the chemisorption of both As(III) and As(V) on the surface of immobilized bacterial cells

Effect of Temperature on Biosorption/Bioaccumulation Kinetic

Temperature is a notable factor controlling the biosorption/bioaccumulation process. The influence of temperature on the of biosorption/bioaccumulation of both As(III) and As(V) by immobilized bacterial cells was carried out from 30 to 50 °C at C_0 is 50 mg/L and SD/MnFe₂O₄ composite loading is 0.9 g/L. A declining biosorption rate of both As(III) and As(V) with increasing temperature from 30 to 50 °C recognized the process to be exothermic (Fig. S9).

Biosorption Activation Energy

Biosorption/bioaccumulation rate constants k_{PSO} of both As(III) and As(V) were estimated from experimental data at different temperatures assuming nonlinear form of pseudo second-order kinetics. Parameters of Arrhenius equation were fitted employing these rate constants for valuing temperature-independent rate parameters and biosorption/bioaccumulation type. A plot of $\ln k_{PSO}$ versus $1/T$ exhibited a straight line with slope $-E_a/R$ (Fig. 5; Table 8). The magnitude of activation energy for As(III) and As(V) biosorption/bioaccumulation on the surface of immobilized bacterial cells were 12.35 and 10.61 kJ/mol, signifying that both the biosorption/bioaccumulation of As(III) and As(V) on the surface of immobilized bacterial cells was activated by chemisorption.

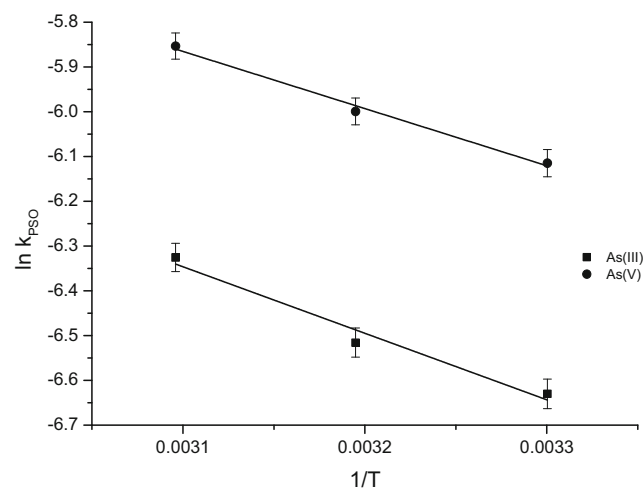


Fig. 5 Determination of the activation energy for As(III) and As(V) biosorption/bioaccumulation on the surface of immobilized bacterial cells (T , 30–50 °C; t , 5–500 min; C_0 , 50 mg/L; pH, 7; M , 0.9 g/L). Error bars represent means \pm standard errors from the mean of duplicate experiments

Table 8 Activation energy for As(III) and As(V) biosorption/bioaccumulation on the surface of immobilized bacterial cells

Inorganic form	T (K)	k_{PSO} (g/mg min)	E_a (kJ/mol)
As(III)	303	1.320E-03	12.355
	313	1.480E-03	
	323	1.790E-03	
As(V)	303	2.210E-03	10.615
	313	2.480E-03	
	323	2.870E-03	

Studies of Influencing Co-existing Ions

The effects of concentrations of initial co-existing ions on the biosorption/bioaccumulation process of As(III) and As(V) on *Corynebacterium glutamicum* MTCC 2745 immobilized on surface of SD/MnFe₂O₄ composite are revealed in Figs. 6a–c and 7a–c, respectively. Consequences clearly showed that the percent removal of As(III) and As(V) were observed to decrease with the presence of a very low concentration of various ions, for example, copper (Cu²⁺), zinc (Zn²⁺), bismuth (Bi³⁺), lead (Pb²⁺), cobalt (Co²⁺), nickel (Ni²⁺), chromium (Cr⁶⁺), and sulfate (SO₄²⁻). On the other hand, in the presence of iron (Fe³⁺) and cadmium (Cd²⁺), the removal efficiencies were observed to increase. The reduction of percent removal in the existence of Cu²⁺, Zn²⁺, Bi³⁺, Pb²⁺, Co²⁺, Ni²⁺, Cr⁶⁺, and SO₄²⁻ ions may be clarified on the basis of the ionic radii. All these ions are bigger than As(III) and As(V), and therefore, in their attendance, the percent removal reduced [52, 53]. This might be owing to the competition of these ions with arsenic for the biosorption sites and/or owing to masking of biosorption sites by the bigger ions [54]. Conversely, the ionic radii of Cd²⁺ and Fe³⁺ are almost the same, so, there was no reducing effect [54]. The percent removal of As(III) and As(V) increased in presence of both Cd²⁺ and Fe³⁺ ions. Mostly Cd²⁺ and Fe³⁺ ions could be biosorbed/bioaccumulated by immobilized bacterial cells and efficiently compensated the surface negative charge generated by specific biosorption/bioaccumulation of As(III) and As(V) and acted as a bridge between immobilized bacterial cells and As(III) and As(V) ions, which has preferred the biosorption/bioaccumulation of As(III) and As(V) anions [52, 55]. While the ionic radius of Cd²⁺ is nearly the same, so there was no reducing effect [53]. As well as this, Fe³⁺ ions being an outstanding adsorbent for arsenic, the current effect in the occurrence of Fe³⁺ may also be owing to adsorption of arsenic on ferric hydroxides (Fe(OH)₃), which would form while Fe³⁺ ions are present in wastewater under oxic conditions [56]. Sulfate is a divalent oxyanion and has competition with anions of both As(III) and As(V) through enhanced electrostatic interaction [57]. Sulfate had an negligible influence on As(III) and

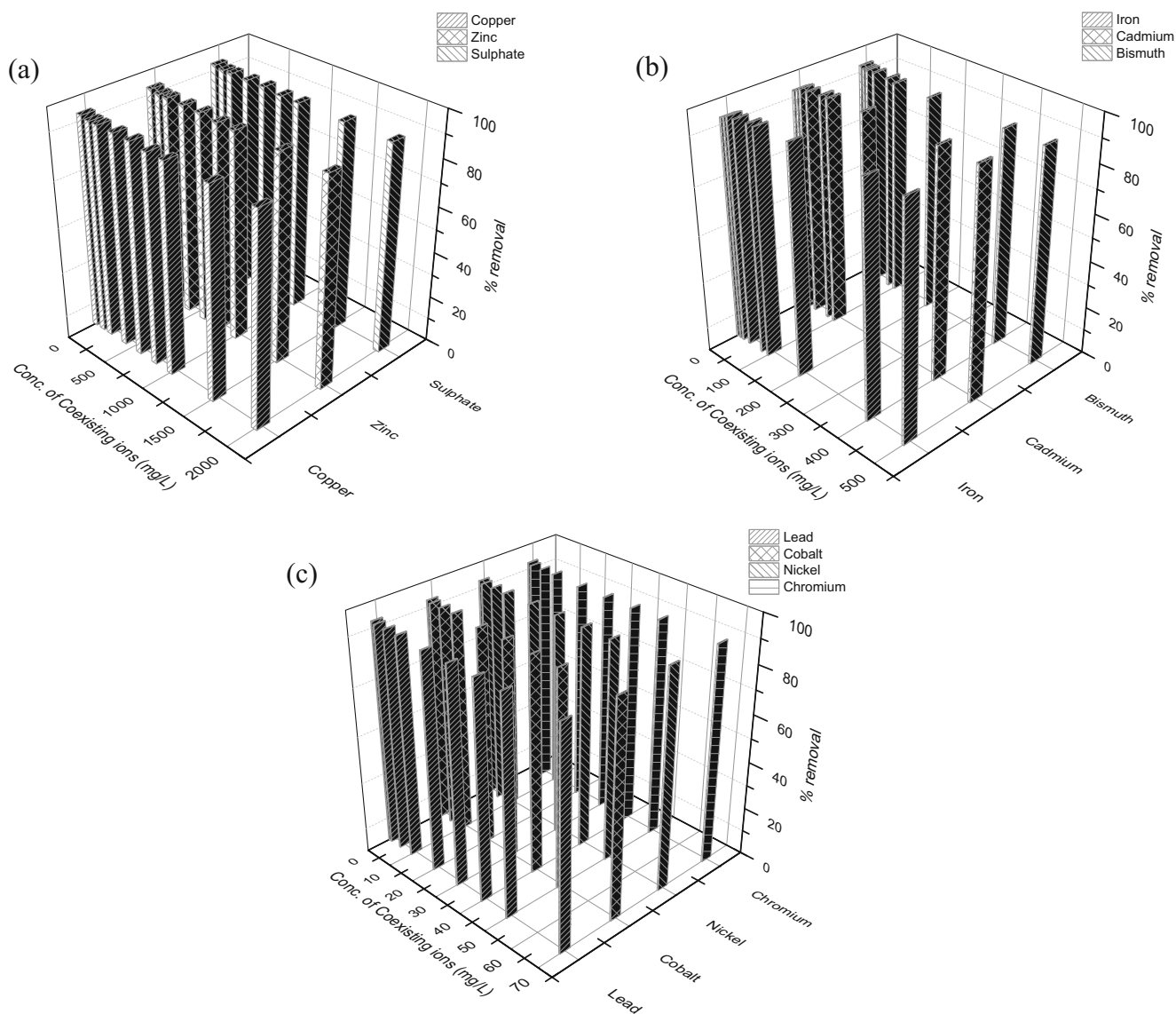


Fig. 6 Effect of co-existing ions **a** copper, zinc, and sulfate; **b** iron, cadmium, and bismuth; and **c** lead, cobalt, nickel, and chromium on the removal of As(III) (C_0 , 50 mg/L; M , 0.9 g/L; pH, 7.0; t , 220 min; T , 30 °C)

As(V) biosorption/bioaccumulation. This is due to the fact that the sulfate binding affinity for the immobilized bacterial cells is much weaker than arsenic [55]. These consequences are also consistent with other study [58, 59].

Characterization

FT-IR Analysis

The biosorption capacity of heavy metal on many biosorbents is governed by the presence of several active functional groups on the surface of biosorbent. The Fourier transform infrared spectra (FT-IR) study of fresh SD/MnFe₂O₄ composite as well as As(III)-acclimatized *B. arsenicus* MTCC 4380 immobilized on surface of SD/MnFe₂O₄ composite at unloaded and metal-loaded stage (Fig. 8a) and fresh SD/MnFe₂O₄ composite plus

As(V)-acclimatized *B. arsenicus* MTCC 4380 immobilized on surface of SD/MnFe₂O₄ composite at unloaded and metal-loaded stage (Fig. 8b) at optimized batch experimental condition was observed for identifying the function groups responsible mainly for the process of biosorption/bioaccumulation. Tables S6 and S7 of the Electronic Supplementary Material specify the wavenumber for the many functional groups present in the fresh SD/MnFe₂O₄ composite and As(III)-acclimatized *B. arsenicus* MTCC 4380 immobilized on surface of SD/MnFe₂O₄ composite at As(III)-unloaded and As(III)-loaded stages and fresh SD/MnFe₂O₄ composite and As(V)-acclimatized *B. arsenicus* MTCC 4380 immobilized on surface of SD/MnFe₂O₄ composite at As(V)-unloaded and As(V)-loaded stages, respectively. Surface –OH and –NH groups were main active functional groups answerable for biosorption/bioaccumulation as the wavenumber shifted from 3432.725 to

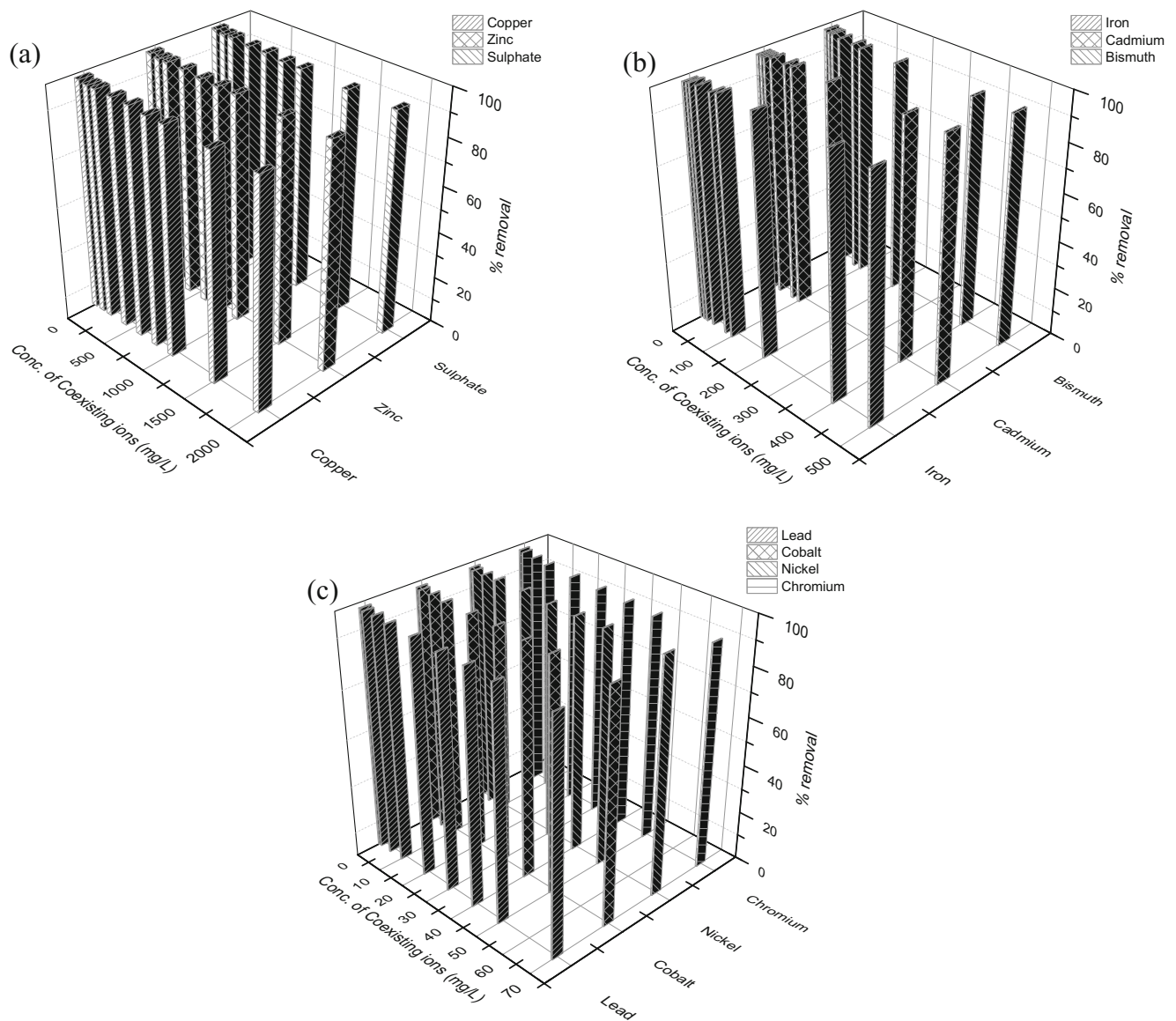


Fig. 7 Effect of co-existing ions **a** copper, zinc, and sulfate; **b** iron, cadmium, and bismuth; and **c** lead, cobalt, nickel, and chromium on the removal of As(V) (C_0 , 50 mg/L; M , 0.9 g/L; pH, 7.0; t , 220 min; T , 30 °C)

3426.977 cm^{-1} (As(III)) and from 3432.725 to 3422.016 cm^{-1} (As(V)) which may be probably owing to the complexation of –OH groups with As(III) or As(V) ions [41]. Some researchers also specified that after the adsorption of arsenic on the Fe–Ce and Fe–Mn adsorbents, the peak of hydroxyl groups reduced or vanished [60, 61]. Aliphatic C–H stretching may be responsible for As(III) and As(V) biosorption/bioaccumulation on As(III) and As(V) acclimatized *B. arsenicus* MTCC 4380 immobilized on surface of SD/MnFe₂O₄ composite as wavenumber shifted from 2929.612 to 2919.69 cm^{-1} and from 2923.602 to 2919.69 cm^{-1} , respectively, possibly owing to the complexation of C–H stretching vibration of alkyl chains [62]. Aldehyde C–H stretching may be responsible for As(III) and As(V) biosorption/bioaccumulation on As(III)- and As(V)-acclimatized

B. arsenicus MTCC 4380 immobilized on surface of SD/MnFe₂O₄ composite as wavenumber shifted from 2854.176 to 2857.674 cm^{-1} and from 2854.176 to 2852.713 cm^{-1} , respectively [63]. Tables S6 and S7 of the Electronic Supplementary Material also display the responsibility of aliphatic acid C=O stretching for As(III) and As(V) biosorption/bioaccumulation by shifting the wavenumber from 1735.647 to 1745.116 cm^{-1} and from 1729.862 to 1735.647 cm^{-1} , respectively [41]. The next biosorption/bioaccumulation peaks at 1640.93 cm^{-1} shifted to 1629.58 cm^{-1} for As(III) and 1640.93 cm^{-1} shifted to 1630.388 cm^{-1} for As(V), perhaps due to the complexation of amide group (N–H stretching and C=O stretching vibration) with As(III) and As(V) ions [64]. Wave number shifted from 1625.426 to 1615.504 cm^{-1} (As(III)) and from 1657.054 to

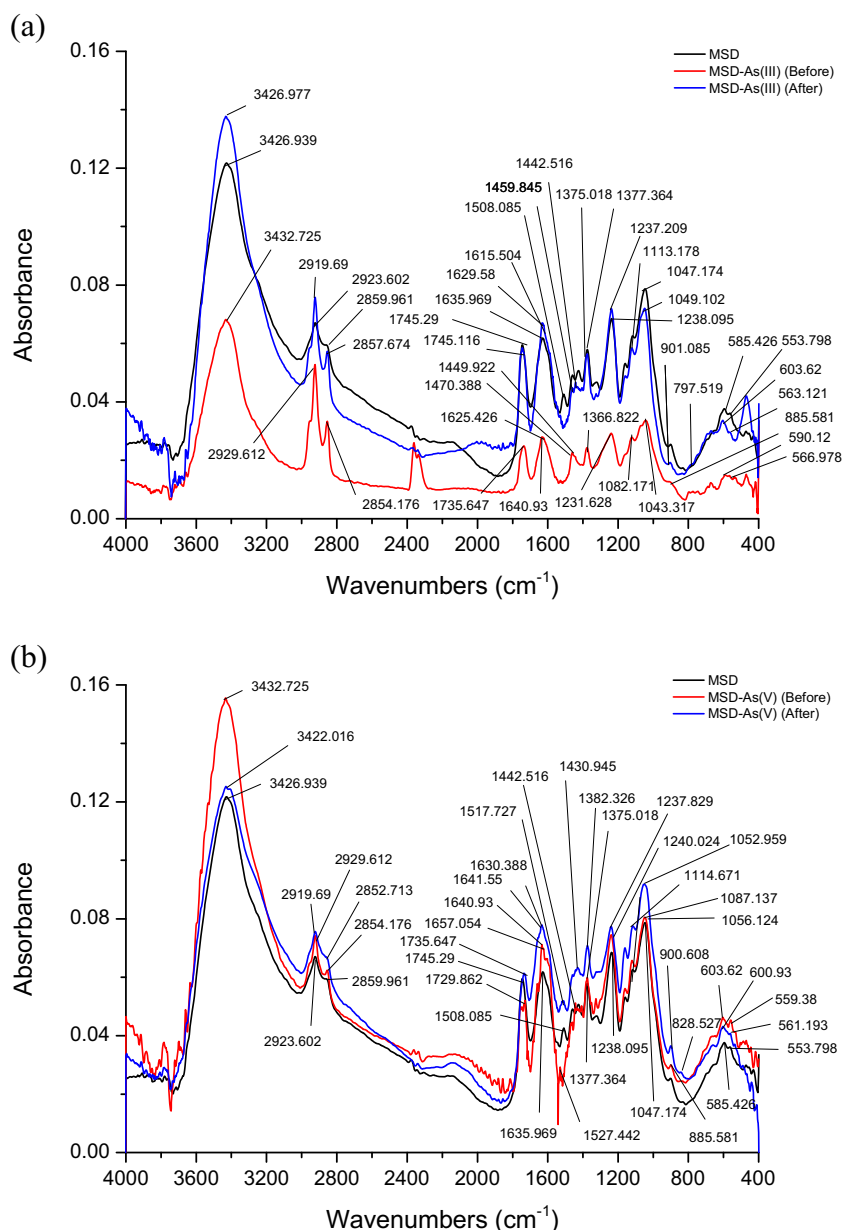


Fig. 8 FT-IR spectra of **a** fresh SD/MnFe₂O₄ composite (MSD), As(III)-acclimatized *B. arsenicus* MTCC 4380 immobilized on SD/MnFe₂O₄ composite before and after As(III) biosorption/bioaccumulation and **b**

fresh SD/MnFe₂O₄ composite (MSD), As(V)-acclimatized *B. arsenicus* MTCC 4380 immobilized on SD/MnFe₂O₄ composite before and after As(V) biosorption/bioaccumulation

1641.55 cm⁻¹ (As(V)) which gave the reactivity of unsaturated group like alkene for the biosorption/bioaccumulation process. Tables S6 and S7 of the Electronic Supplementary Material also exhibit the intense bands at 1470.388 cm⁻¹ which shifted to 1459.845 cm⁻¹ (As(III)) and at 1527.442 cm⁻¹, shifted to 1517.727 cm⁻¹ (As(V)) that indicated the responsibility of aromatic -NO₂ group for the biosorption/bioaccumulation process, respectively. Another shift was detected from 1449.922 to 1442.516 cm⁻¹ (As(III)) and from 1442.516 to 1430.945 cm⁻¹ (As(V)), corresponding to the complexation of nitrogen with As(III) and As(V) ions of the N-H group [65]. Wavenumber shifted from 1366.822 to 1375.018 cm⁻¹ (As(III)) and from

1375.018 to 1382.326 cm⁻¹ (As(V)) assigned the reactivity of carboxylate anion C=O stretching for the biosorption/bioaccumulation process [53]. Wavenumber 1231.628 cm⁻¹ shifted to 1237.209 cm⁻¹ and 1240.024 cm⁻¹ shifted to 1237.829 cm⁻¹ assigned for -SO₃ stretching for the biosorption/bioaccumulation of As(III) and As(V), respectively. The peaks at 1082.1705 cm⁻¹ (As(III)) and 1087.132 cm⁻¹ As(V) may be attributed to the C-N stretching vibrations of amino groups which shifted to higher frequency and appeared at 1113.178 and 1114.671 cm⁻¹, respectively, due to the interaction of nitrogen from the amino group with As(III) and As(V) ions [66]. Wavenumber 1043.317 cm⁻¹ shifted to

1049.102 cm^{-1} (As(III)) and shifting from 1056.124 to 1052.959 cm^{-1} (As(V)) indicated the Si–O stretching, active for the biosorption/bioaccumulation process. The other weak biosorption/bioaccumulation peak shifted from 885.581 to 901.085 cm^{-1} (As(III)) and from 885.581 to 900.608 cm^{-1} , corresponding to the O–C–O scissoring vibration of polysaccharide [67]. The band at 590.12 cm^{-1} (Fig. 8a) and 603.62 cm^{-1} (Fig. 8b) could be attributed to the existence of Fe–O bond [68], but then it shifted to 603.62 cm^{-1} after biosorption/bioaccumulation of As(III) (Fig. 8a) and to 600.93 cm^{-1} after biosorption/bioaccumulation of As(V) (Fig. 8b), respectively. A typical peak at 566.978 cm^{-1} (Fig. 8a) and 559.38 cm^{-1} (Fig. 8b) could be assigned to Mn–O bond [69] and it had a different variability to 563.121 cm^{-1} (Fig. 1a) and 561.193 cm^{-1} (Fig. 8b) for biosorption/bioaccumulation of As(III) and As(V), respectively. The change in wavenumber of Me–O bonds after biosorption/bioaccumulation of As(III) and As(V) indicated that both Fe–O and Mn–O bonds were responsible for both MnFe_2O_4 –As(III) and MnFe_2O_4 –As(V) [68, 70]. Presence of As(III) and As(V) on the As(III) and As(V) acclimatized *B. arsenicus* MTCC 4380 immobilized on surface of SD/ MnFe_2O_4 composite can be assured from the bands appeared at 797.519 cm^{-1} (Fig. 8a) and 828.527 cm^{-1} (Fig. 8b), respectively [71]. It has to be cited here, that a clear band was very hard to be got in the case of As(III), compared with the distinctive band of As(III) found at 797.519 cm^{-1} and As(V) found at 828.527 cm^{-1} . This may be because of different mechanisms involved in As(III) and As(V) biosorption/bioaccumulation. It should be distinguished that the As–O band after biosorption/bioaccumulation of arsenic was not clearly observed because of the broad overlapping peaks in this region [70].

SEM-EDX Analysis

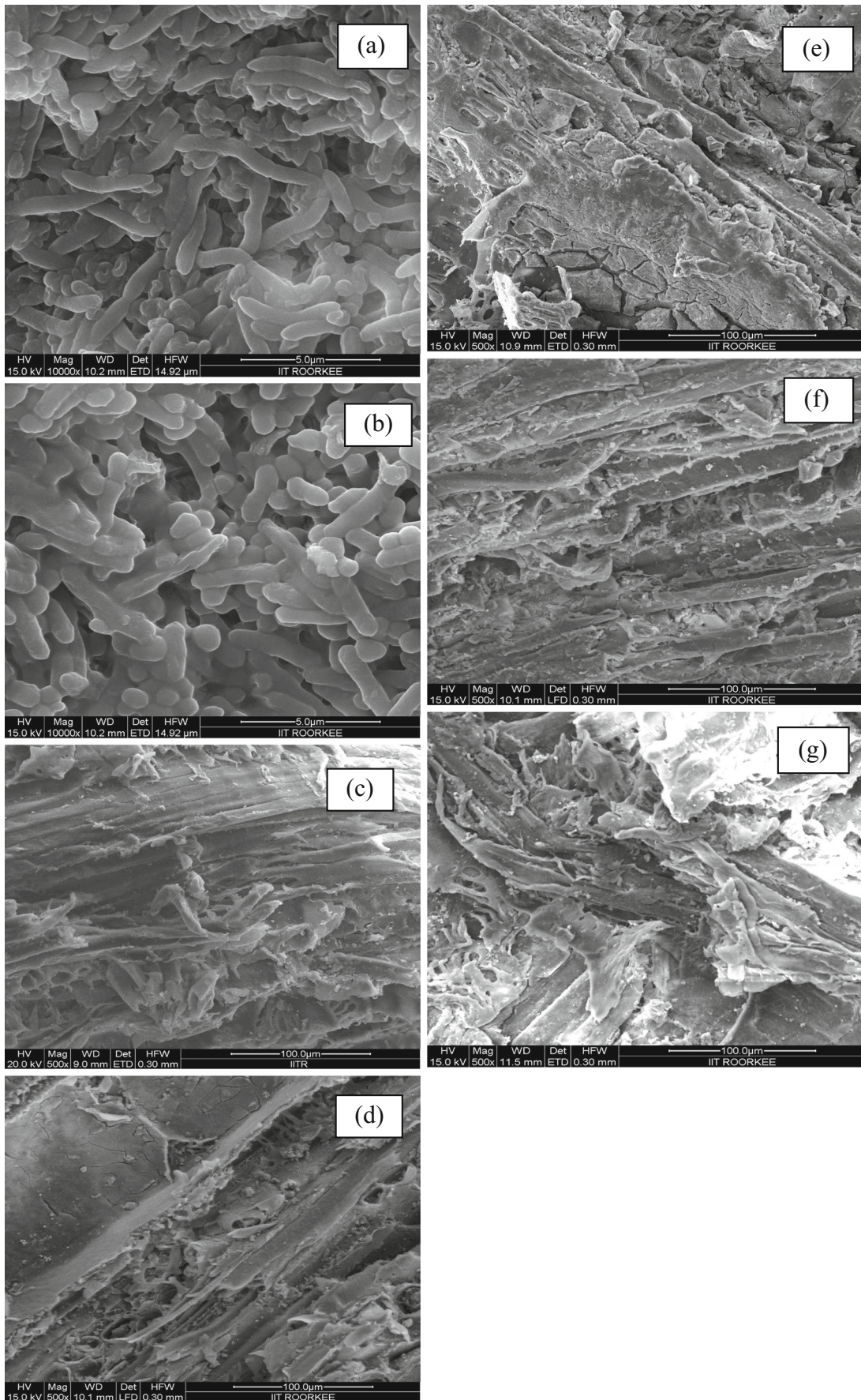
Figure 9a, b exhibits the morphology of As(III) and As(V) acclimatized living bacterial cells of *B. arsenicus* MTCC 4380, respectively. From the figure, it is obvious that they were basically rod-like shape. The SEM images of the prepared fresh SD/ MnFe_2O_4 composite (Fig. 9c) and As(III) acclimatized the *B. arsenicus* MTCC 4380 immobilized on surface of SD/ MnFe_2O_4 composite at stage of unloaded and loaded with As(III) (Fig. 9d, e) and As(V) acclimatized the *B. arsenicus* MTCC 4380 immobilized on surface of SD/ MnFe_2O_4 composite at stage of unloaded and loaded with As(V) (Fig. 9f, g) were also shown. It can be understood from Fig. 9c, manganese ferrite (MnFe_2O_4) particles with numerous diameters were arbitrarily distributed on the acid treated SD surface. It is clear from Fig. 9d, f that most of the active sites of SD/ MnFe_2O_4 composite were shielded owing to the formation of biofilm on it. The bacterial mass partially occupies the void spaces of the biosorbent surface, so formation of biolayer on the surface of biosorbent decreases its surface porosity [72]. It can be observed from Fig. 9e, g that the immobilized bacterial cells

Fig. 9 Scanning electron micrographs (SEM) of **a** As(III)-acclimatized living cells of *B. arsenicus* MTCC 4380, **b** As(V)-acclimatized living cells of *B. arsenicus* MTCC 4380 (original magnification, $\times 10000$), **c** fresh SD/ MnFe_2O_4 composite, **d** As(III)-acclimatized *B. arsenicus* MTCC 4380 immobilized on SD/ MnFe_2O_4 composite at unloaded stage, **e** As(III)-acclimatized *B. arsenicus* MTCC 4380 immobilized on SD/ MnFe_2O_4 composite at loaded stage, **f** As(V)-acclimatized *B. arsenicus* MTCC 4380 immobilized on SD/ MnFe_2O_4 composite at unloaded stage, and **g** As(V)-acclimatized *B. arsenicus* MTCC 4380 immobilized on SD/ MnFe_2O_4 composite at loaded stage (original magnification, $\times 500$)

have bulky structure with no porosity. A change in surface morphology from being smooth to rough and occupation of pores specified the As(III) and As(V) biosorption/bioaccumulation on the surface and pores of SD/ MnFe_2O_4 composite providing it a rough texture (Fig. 9e, g) [73].

Conclusions

- The current study showed that the *B. arsenicus* MTCC 4380 immobilized on surface of SD/ MnFe_2O_4 composite was applied fruitfully for the biosorption/bioaccumulation of both As(III) and As(V) from synthetically prepared wastewater.
- The optimum contact time and temperature for biosorption/bioaccumulation of both As(III) and As(V) were 220 min and 30 °C, respectively.
- Contact time desirable for achievement of equilibrium improved with increasing concentration, though remained virtually unaffected by increasing temperature.
- The rate of biosorption/bioaccumulation of both As(III) and As(V) by immobilized bacterial cells decreased with increasing concentration.
- By applying 14 different kinetic models and using method of the nonlinear regression for curve fitting analysis (maximizing the correlation coefficient (R , R^2 , and $\overline{R^2}$) and minimizing the error values (SSE, reduced χ^2 , and root-MSE)) to evaluate optimum parameter sets, Brouers–Weron–Sotolongo as well as Avrami models were found suitable to predict the kinetic of biosorption/bioaccumulation of both As(III) and As(V) on the surface of immobilized bacterial cells according to GoFM values.
- The current experimental data also followed pseudo second-order model very well, hence it can be concluded that chemisorption was the possible route of biosorption/bioaccumulation on immobilized bacterial cells.
- The results achieved from different mechanistic models indicated the controller of film diffusion over pore diffusion.
- The effective diffusivity estimated by using Vermeulen's approximation was indicated that the interaction between



arsenic ions (either As(III) or As(V)) and immobilized bacterial cells were chemical in nature.

- The related thermodynamic parameters revealed that the biosorption/bioaccumulation of both As(III) and As(V) had been a feasible and exothermic process and spontaneous.
- From Arrhenius equation, it was confirmed that the mechanism of biosorption/bioaccumulation of As(III) and As(V) by immobilized bacterial cells might be an ion exchange type.
- EDX analysis documented the attendance of iron and manganese in the SD/MnFe₂O₄ composite, and it also established the fact that both As(III) and As(V) was biosorbed/bioaccumulated on the immobilized bacterial cells.
- Spectroscopic studies (Fe-SEM and FT-IR) confirmed that ion exchange process was responsible for the uptake of arsenic (As(III) or As(V)) on immobilized bacterial cells.
- *B. arsenicus* MTCC 4380 immobilized on surface of SD/MnFe₂O₄ composite can be used as a capable biosorbent for removal of both As(III) and As(V) from contaminated water sources.

Nomenclature

a_E Elovich coefficient representing the initial adsorption rate (mg/g min)

b_E Elovich coefficient representing desorption constant (g/mg)

A the frequency factor

B_{bt} a mathematical function of F ($F = q_t/q_e$)

C_0 initial concentration of arsenic in the solution (mg/L)

C_e equilibrium concentration of arsenic in the solution (mg/L)

C_s the concentration of arsenic on the biosorbent and in the solution (mg/L)

C_{int} the intercept of the intraparticle diffusion plot (mg/g)

d the thickness of the water film adhered to the biosorbent (cm)

D_1 film diffusion constant (cm²/s)

D_2 pore diffusion constant (cm²/s)

D_e diffusivity (m²/s)

D_f film diffusion coefficient (cm²/s)

D_p pore diffusion coefficient (cm²/s)

E_a the activation energy of adsorption (kJ/mol)

F the adsorption progress ($F = q_t/q_e$)

f_2 the involvement of pseudo second-order model

h the initial sorption rate (mg/g min)

k_{AV} the Avrami kinetic rate coefficient (1/min)

k_b the Bangham model constant (L/g)

k_d the equilibrium constant (L/g),

k_{DW} the Dumwald–Wagner rate constant (1/min)

k_{EXP} the exponential rate coefficient (mg/g min)

k_{int} the intraparticle diffusion rate coefficient (mg/g min^{0.5})

k_M the film diffusion rate constant (1/min)

k_{MOE} the mixed 1,2-order rate coefficient (1/min)

$k_{nBWS, \alpha}$ the Brouers–Weron–Sotolongo reaction constant (1/min)

k_{PF} the fractional power model rate coefficient (mg/g min)

k_{PFO} the pseudo first-order rate coefficient (1/min)

k_{PSO} the pseudo second-order rate coefficient (g/mg min)

$k'_{1,0}$ the fractal-like mixed 1,2-order rate coefficient (1/min)^α

k'_{2R} the modified second-order rate coefficient (1/min)

k''_{2R} the Ritchie second-order rate coefficient (1/min)

k'_{EXP} division of k_{EXP} by q_e (1/min)

k''_{EXP} the fractal-like exponential rate coefficient (1/min)^α

k'_{PFO} the fractal-like pseudo first-order kinetic rate coefficient (1/min)^α

$k'_{F PSO}$ is the fractal-like pseudo second-order kinetic rate coefficient (g/mg min)^α

k'_{PSO} multiplication of q_e and k_{PSO} (1/min)

$k''_{F PSO}$ multiplication of q_e and $k'_{F PSO}$ (1/min)

m the weight of the biosorbent per liter of solution (g/L)

m_b an integer

n the number of observations in the experimental study

n_{AV} constant corresponding to the mechanism of adsorption

n_{BWS} a fractional reaction order

n_R number of surface sites

p the number of parameters to be estimated

q_e the amount of adsorbate adsorbed on the biosorbent surface at equilibrium (mg/g)

q_t the amount of adsorbate adsorbed on the biosorbent surface at time t (mg/g)

r mean radius of biosorbent particle (cm)

R the universal gas constant (8.314 J/mol K)

R_e percent removal of adsorbate

t contact time (min)

t^α a fractal time

T the solution temperature (K)

v adjustment parameter

V the volume of the solution (mL)

Greek symbols

α the fractal time exponent

α_b Bangham model constant

θ the biosorbent surface coverage at pre-adsorbed stage, ($\theta = q_t/q_e$) dimensionless

θ_0 the biosorbent surface coverage at time t , ($\theta_0 = q_0/q_e$) dimensionless

θ_e the equilibrium surface coverage

$\tau_{1/2}$ half-reaction time (min)

$\tau_{nBWS, \alpha}$ the time required for adsorbing half the maximum amount

ΔG^0 Gibbs free energy change (kJ/mol)

ΔH^0 enthalpy change (kJ/mol)

ΔS^0 entropy change (J/mol K)

Acknowledgments Our thanks to the Indian Institute of Technology, Roorkee for providing necessary facilities and to the Ministry of Human Resource Development, Government of India for financial support. The thoughtful comments by Dr. Apostolos Giannis, the Editor, and two anonymous reviewers are highly appreciated.

References

- Mondal P, Majumder CB, Mohanty B (2006) Laboratory based approaches for arsenic remediation from contaminated water: recent developments. *J Hazard Mater* 137(1):464–479. doi:10.1016/j.jhazmat.2006.02.023
- Smedley PL, Kinniburgh DG (2002) A review of the source, behaviour and distribution of arsenic in natural waters. *Appl Geochem* 17(5):517–568. doi:10.1016/S0883-2927(02)00018-5
- Basha CA, Bhadrinarayana NS, Anantharaman N, Begum KM (2008) Heavy metal removal from copper smelting effluent using electrochemical cylindrical flow reactor. *J Hazard Mater* 152(1):71–78. doi:10.1016/j.jhazmat.2007.06.069
- Mohan D, Pittman CU (2007) Arsenic removal from water/wastewater using adsorbents—a critical review. *J Hazard Mater* 142(1):1–53. doi:10.1016/j.jhazmat.2007.01.006
- WHO (1993) Guidelines for drinking water quality. World Health Organization, Geneva, p 41
- European Commission Directive (1998) 98/83/EC, related with drinking water quality intended for human consumption, Brussels, Belgium
- Emett MT, Khoe GH (2001) Photochemical oxidation of arsenic by oxygen and iron in acidic solutions. *Water Res* 35(3):649–656. doi:10.1016/S0043-1354(00)00294-3
- Nguyen VT, Vigneswaran S, Ngo HH, Shon HK, Kandasamy J (2009) Arsenic removal by a membrane hybrid filtration system. *Desalination* 236(1):363–369. doi:10.1016/j.desal.2007.10.088
- Chutia P, Kato S, Kojima T, Satokawa S (2009) Arsenic adsorption from aqueous solution on synthetic zeolites. *J Hazard Mater* 162(1):440–447. doi:10.1016/j.jhazmat.2008.05.061
- Shao W, Li X, Cao Q, Luo F, Li J, Du Y (2008) Adsorption of arsenate and arsenite anions from aqueous medium by using metal (III)-loaded amberlite resins. *Hydrometallurgy* 91(1):138–143. doi:10.1016/j.hydromet.2008.01.005
- Malik A (2004) Metal bioremediation through growing cells. *Environ Int* 30(2):261–278. doi:10.1016/j.envint.2003.08.001
- Naja G, Volesky B (2006) Behavior of the mass transfer zone in a biosorption column. *Environ Sci Technol* 40(12):3996–4003. doi:10.1021/es051542p
- Le Cloirec P, André Y, Faur-Brasquet C, Gerente C (2003) Engineered biofilms for metal ion removal. *Rev Environ Sci Biotechnol* 2(2-4):177–192
- Mondal P, Majumder CB, Mohanty B (2008) Treatment of arsenic contaminated water in a batch reactor by using *Ralstonia eutropha* MTCC 2487 and granular activated carbon. *J Hazard Mater* 153(1):588–599. doi:10.1016/j.jhazmat.2007.09.028
- Shao L, Ren Z, Zhang G, Chen L (2012) Facile synthesis, characterization of a MnFe₂O₄/activated carbon magnetic composite and its effectiveness in tetracycline removal. *Mater Chem Phys* 135(1):16–24. doi:10.1016/j.matchemphys.2012.03.035
- Bianfang Z, Guide T, Zonglin Y, Zhenbiao W, Qingfen Y, Jianpo C (2007) Synthesis of magnetic manganese ferrite. *J Wuhan Univ Technol Mater Sci Ed* 22:514–517
- Hadi M, McKay G, Samarghandi MR, Maleki A, Solaimany Aminabad M (2012) Prediction of optimum adsorption isotherm: comparison of Chi-square and Log-likelihood statistics. *Desalin Water Treat* 49(1-3):81–94. doi:10.1080/19443994.2012.708202
- Hanna OT, Sandall OC (1995) Computational methods in chemical engineering. Prentice-Hall International, New Jersey
- Warrens MJ (2008) On similarity coefficients for 2 × 2 tables and correction for chance. *Psychometrika* 73(3):487–502. doi:10.1007/s11336-008-9059-y
- Haerifar M, Azizian S (2013) An exponential kinetic model for adsorption at solid/solution interface. *Chem Eng J* 215–216:65–71. doi:10.1016/j.cej.2012.11.017
- Qiu H, Lv L, Pan BC, Zhang QJ, Zhang WM, Zhang QX (2009) Critical review in adsorption kinetic models. *J Zhejiang Univ Sci A* 10(5):716–724
- Singh TS, Pant KK (2006) Kinetics and mass transfer studies on the adsorption of arsenic onto activated alumina and iron oxide impregnated activated alumina. *Water Qual Res J Can* 41(2):147–156
- Al-Degs YS, El-Barghouthi MI, El-Sheikh AH, Walker GM (2008) Effect of solution pH, ionic strength, and temperature on adsorption behavior of reactive dyes on activated carbon. *Dyes Pigments* 77(1):16–23. doi:10.1016/j.dyepig.2007.03.001
- Mondal P, Mohanty B, Majumder CB (2009) Treatment of simulated arsenic contaminated groundwater using GAC-Cu in batch reactor: optimization of process parameters. *Can J Chem Eng* 87(5):766–778. doi:10.1002/cjce.20214
- Mondal P, Balo Majumder C, Mohanty B (2007) Removal of trivalent arsenic (As (III)) from contaminated water by calcium chloride (CaCl₂)-impregnated rice husk carbon. *Ind Eng Chem Res* 46(8):2550–2557. doi:10.1021/ie060702i
- Mondal P, Mohanty B, Balomajumder C (2010) Treatment of arsenic contaminated groundwater using calcium impregnated granular activated carbon in a batch reactor: optimization of process parameters. *CLEAN-Soil, Air, Water* 38(2):129–139. doi:10.1002/clen.200900081
- Tian Y, Wu M, Lin X, Huang P, Huang Y (2011) Synthesis of magnetic wheat straw for arsenic adsorption. *J Hazard Mater* 193:10–16. doi:10.1016/j.jhazmat.2011.04.093
- Mishra V, Balomajumder C, Agarwal VK (2010) Zn (II) ion biosorption onto surface of eucalyptus leaf biomass: isotherm, kinetic, and mechanistic modeling. *CLEAN-Soil, Air, Water* 38(11):1062–1073. doi:10.1002/clen.201000030
- Mishra V, Balomajumder C, Agarwal VK (2013) Design and optimization of simultaneous biosorption and bioaccumulation (SBB) system: a potential method for removal of Zn (II) ion from liquid phase. *Desalin Water Treat* 51(16-18):3179–3188. doi:10.1080/19443994.2012.749027
- Ranjan D, Talat M, Hasan SH (2009) Biosorption of arsenic from aqueous solution using agricultural residue 'rice polish'. *J Hazard Mater* 166(2):1050–1059. doi:10.1016/j.jhazmat.2008.12.013
- Ncibi MC, Ranguin R, Pintor MJ, Jeanne-Rose V, Sillanpää M, Gaspard S (2014) Preparation and characterization of chemically activated carbons derived from Mediterranean *Posidonia oceanica* (L.) fibres. *J Anal Appl Pyrolysis* 109:205–214. doi:10.1016/j.jaap.2014.06.010
- Vaghehti JC, Lima EC, Royer B, da Cunha BM, Cardoso NF, Brasil JL, Dias SL (2009) Pecan nutshell as biosorbent to remove Cu (II), Mn (II) and Pb (II) from aqueous solutions. *J Hazard Mater* 162(1):270–280. doi:10.1016/j.jhazmat.2008.05.039
- Cheung CW, Porter JF, McKay G (2001) Sorption kinetic analysis for the removal of cadmium ions from effluents using bone char. *Water Res* 35(3):605–612. doi:10.1016/S0043-1354(00)00306-7
- Haerifar M, Azizian S (2012) Fractal-like adsorption kinetics at the solid/solution interface. *J Phys Chem C* 116(24):13111–13119. doi:10.1021/jp301261h

35. Miretzky P, Muñoz C, Carrillo-Chávez A (2008) Experimental binding of lead to a low cost on biosorbent: Nopal (*Opuntia streptacantha*). *Bioresour Technol* 99(5):1211–1217. doi:10.1016/j.biortech.2007.02.045
36. Lu S, Gibb SW (2008) Copper removal from wastewater using spent-grain as biosorbent. *Bioresour Technol* 99(6):1509–1517. doi:10.1016/j.biortech.2007.04.024
37. Kavitha D, Namasivayam C (2007) Experimental and kinetic studies on methylene blue adsorption by coir pith carbon. *Bioresour Technol* 98(1):14–21. doi:10.1016/j.biortech.2005.12.008
38. Rengaraj S, Yeon JW, Kim Y, Jung Y, Ha YK, Kim WH (2007) Adsorption characteristics of Cu (II) onto ion exchange resins 252H and 1500H: kinetics, isotherms and error analysis. *J Hazard Mater* 143(1):469–477. doi:10.1016/j.jhazmat.2006.09.064
39. Atun G, Hisarlı G (2003) Adsorption of carminic acid, a dye onto glass powder. *Chem Eng J* 95(1):241–249. doi:10.1016/S1385-8947(03)00110-4
40. Weber WJ, Morris JC (1963) Intraparticle diffusion during the sorption of surfactants onto activated carbon. *J Sanit Eng Div Am Soc Civ Eng* 89(1):53–61
41. Singha B, Das SK (2011) Biosorption of Cr (VI) ions from aqueous solutions: kinetics, equilibrium, thermodynamics and desorption studies. *Colloids Surf B* 84(1):221–232. doi:10.1016/j.colsurfb.2011.01.004
42. Nouri L, Ghodbane I, Hamdaoui O, Chiha M (2007) Batch sorption dynamics and equilibrium for the removal of cadmium ions from aqueous phase using wheat bran. *J Hazard Mater* 149(1):115–125. doi:10.1016/j.jhazmat.2007.03.055
43. Shivaji S, Suresh K, Chaturvedi P, Dube S, Sengupta S (2005) *Bacillus arsenicus* sp. nov., an arsenic-resistant bacterium isolated from a siderite concretion in West Bengal, India. *Int J Syst Evol Microbiol* 55(3):1123–1127. doi:10.1099/ijs.0.63476-0
44. Sag Y, Kutsal T (1995) Biosorption of heavy metals by *Zoogloea ramigera*: use of adsorption isotherms and a comparison of biosorption characteristics. *Chem Eng J* 60(1):181–188. doi:10.1016/0923-0467(95)03014-X
45. Green-Ruiz C, Rodriguez-Tirado V, Gomez-Gil B (2008) Cadmium and zinc removal from aqueous solutions by *Bacillus jeotgali*: pH, salinity and temperature effects. *Bioresour Technol* 99(9):3864–3870. doi:10.1016/j.biortech.2007.06.047
46. Kacar Y, Arpa Ç, Tan S, Denizli A, Genç Ö, Arica MY (2002) Biosorption of Hg (II) and Cd (II) from aqueous solutions: comparison of biosorptive capacity of alginate and immobilized live and heat inactivated *Phanerochaete chrysosporium*. *Process Biochem* 37(6):601–610. doi:10.1016/S0032-9592(01)00248-5
47. Özdemir S, Kilinc E, Poli A, Nicolaus B, Güven K (2009) Biosorption of Cd, Cu, Ni, Mn and Zn from aqueous solutions by thermophilic bacteria, *Geobacillus toebii* sub. sp. *decanicus* and *Geobacillus thermoleovorans* sub. sp. *stromboliensis*: equilibrium, kinetic and thermodynamic studies. *Chem Eng J* 152(1):195–206. doi:10.1016/j.cej.2009.04.041
48. Meena AK, Mishra GK, Rai PK, Rajagopal C, Nagar PN (2005) Removal of heavy metal ions from aqueous solutions using carbon aerogel as an adsorbent. *J Hazard Mater* 122(1):161–170. doi:10.1016/j.jhazmat.2005.03.024
49. Roy P, Mondal NK, Das K (2014) Modeling of the adsorptive removal of arsenic: a statistical approach. *J Environ Chem Eng* 2(1):585–597. doi:10.1016/j.jece.2013.10.014
50. Ngah WW, Hanafiah MA (2008) Adsorption of copper on rubber (*Hevea brasiliensis*) leaf powder: kinetic, equilibrium and thermodynamic studies. *Biochem Eng J* 39(3):521–530. doi:10.1016/j.bej.2007.11.006
51. Crini G, Badot PM (2008) Application of chitosan, a natural aminopolysaccharide, for dye removal from aqueous solutions by adsorption processes using batch studies: a review of recent literature. *Prog Polym Sci* 33(4):399–447. doi:10.1016/j.progpolymsci.2007.11.001
52. Pandey PK, Choubey S, Verma Y, Pandey M, Chandrashekhar K (2009) Biosorptive removal of arsenic from drinking water. *Bioresour Technol* 100(2):634–637. doi:10.1016/j.biortech.2008.07.063
53. Baig JA, Kazi TG, Shah AQ, Kandhro GA, Afridi HI, Khan S, Kolachi NF (2010) Biosorption studies on powder of stem of *Acacia nilotica*: removal of arsenic from surface water. *J Hazard Mater* 178(1):941–948. doi:10.1016/j.jhazmat.2010.02.028
54. Maliyekkal SM, Philip L, Pradeep T (2009) As (III) removal from drinking water using manganese oxide-coated-alumina: performance evaluation and mechanistic details of surface binding. *Chem Eng J* 153(1):101–107. doi:10.1016/j.cej.2009.06.026
55. Zhang G, Liu H, Liu R, Qu J (2009) Adsorption behavior and mechanism of arsenate at Fe–Mn binary oxide/water interface. *J Hazard Mater* 168(2):820–825. doi:10.1016/j.jhazmat.2009.02.137
56. Kundu S, Gupta AK (2006) Adsorptive removal of As (III) from aqueous solution using iron oxide coated cement (IOCC): evaluation of kinetic, equilibrium and thermodynamic models. *Sep Purif Technol* 51(2):165–172. doi:10.1016/j.seppur.2006.01.007
57. Awual MR, Jyo A, Ihara T, Seko N, Tamada M, Lim KT (2011) Enhanced trace phosphate removal from water by zirconium (IV) loaded fibrous adsorbent. *Water Res* 45(15):4592–4600. doi:10.1016/j.watres.2011.06.009
58. Balaji T, Yokoyama T, Matsunaga H (2005) Adsorption and removal of As (V) and As (III) using Zr-loaded lysine diacetic acid chelating resin. *Chemosphere* 59(8):1169–1174. doi:10.1016/j.chemosphere.2004.12.007
59. Chiban M, Carja G, Lehtu G, Sinan F (2011) Equilibrium and thermodynamic studies for the removal of As (V) ions from aqueous solution using dried plants as adsorbents. *Arab J Chem*. doi:10.1016/j.arabjc.2011.10.002
60. Zhang Y, Yang M, Dou XM, He H, Wang DS (2005) Arsenate adsorption on an Fe-Ce bimetal oxide adsorbent: role of surface properties. *Environ Sci Technol* 39(18):7246–7253. doi:10.1021/es050775d
61. Zhang GS, Qu JH, Liu HJ, Liu RP, Li GT (2007) Removal mechanism of As (III) by a novel Fe–Mn binary oxide adsorbent: oxidation and sorption. *Environ Sci Technol* 41(13):4613–4619. doi:10.1021/es063010u
62. Sari A, Tuzen M (2009) Biosorption of As (III) and As (V) from aqueous solution by macrofungus (*Inonotus hispidus*) biomass: equilibrium and kinetic studies. *J Hazard Mater* 164(2):1372–1378. doi:10.1016/j.jhazmat.2008.09.047
63. Tuzen M, Sari A, Mendil D, Uluozlu OD, Soylak M, Dogan M (2009) Characterization of biosorption process of As (III) on green algae *Ulothrix cylindricum*. *J Hazard Mater* 165(1):566–572. doi:10.1016/j.jhazmat.2008.10.020
64. Seki H, Suzuki A, Maruyama H (2005) Biosorption of chromium (VI) and arsenic (V) onto methylated yeast biomass. *J Colloid Interface Sci* 281(2):261–266. doi:10.1016/j.jcis.2004.08.167
65. François F, Lombard C, Guigner JM, Soreau P, Brian-Jaisson F, Martino G, Vandervennet M, Garcia D, Molinier AL, Pignol D, Peduzzi J (2012) Isolation and characterization of environmental bacteria capable of extracellular biosorption of mercury. *Appl Environ Microbiol* 78(4):1097–1106. doi:10.1128/AEM.06522-11
66. Giri AK, Patel RK, Mahapatra SS (2011) Artificial neural network (ANN) approach for modelling of arsenic (III) biosorption from aqueous solution by living cells of *Bacillus cereus* biomass. *Chem Eng J* 178:15–25. doi:10.1016/j.cej.2011.09.111
67. Pokhrel D, Viraraghavan T (2007) Arsenic removal from an aqueous solution by modified *A. niger* biomass: batch kinetic and isotherm studies. *J Hazard Mater* 150(3):818–825. doi:10.1016/j.jhazmat.2007.05.041

68. Ren Y, Li N, Feng J, Luan T, Wen Q, Li Z, Zhang M (2012) Adsorption of Pb (II) and Cu (II) from aqueous solution on magnetic porous ferrosinell $MnFe_2O_4$. *J Colloid Interface Sci* 367(1): 415–421. doi:10.1016/j.jcis.2011.10.022
69. Parida KM, Mallick S, Mohapatra BK, Misra VN (2004) Studies on manganese-nodule leached residues: 1. Physicochemical characterization and its adsorption behavior toward Ni^{2+} in aqueous system. *J Colloid Interface Sci* 277(1):48–54. doi:10.1016/j.jcis.2004.04.057
70. Li Z, Deng S, Yu G, Huang J, Lim VC (2010) As (V) and As (III) removal from water by a Ce–Ti oxide adsorbent: behavior and mechanism. *Chem Eng J* 161(1):106–113. doi:10.1016/j.cej.2010.04.039
71. Aryal M, Ziagova M, Liakopoulou-Kyriakides M (2010) Study on arsenic biosorption using Fe (III)-treated biomass of *Staphylococcus xylosus*. *Chem Eng J* 162(1):178–185. doi:10.1016/j.cej.2010.05.026
72. Mondal P, Majumder CB, Mohanty B (2008) Treatment of arsenic contaminated water in a batch reactor by using *Ralstonia eutropha* MTCC 2487 and granular activated carbon. *J Hazard Mater* 153(1):588–599. doi:10.1016/j.jhazmat.2007.09.028
73. Agarwal B, Balomajumder C, Thakur PK (2013) Simultaneous co-adsorptive removal of phenol and cyanide from binary solution using granular activated carbon. *Chem Eng J* 228:655–664. doi:10.1016/j.cej.2013.05.030